NASA/TM-2005-213778

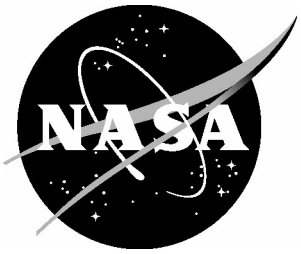

Assessment of Technologies for the Space Shuttle External Tank Thermal Protection System and Recommendations for Technology Improvement

Part 3: Material Property Characterization, Analysis, and Test Methods

Thomas S. Gates, Theodore F. Johnson, and Karen S. Whitley
Langley Research Center, Hampton, Virginia

July 2005

NASA/TM-2005-213778

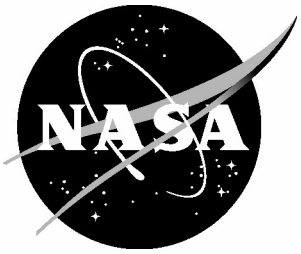

Assessment of Technologies for the Space Shuttle External Tank Thermal Protection System and Recommendations for Technology Improvement

Part 3: Material Property Characterization, Analysis, and Test Methods

Thomas S. Gates, Theodore F. Johnson, and Karen S. Whitley
Langley Research Center, Hampton, Virginia

National Aeronautics and
Space Administration

Langley Research Center
Hampton, Virginia 23681-2199

July 2005

The NASA STI Program Office . . . in Profile

Since its founding, NASA has been dedicated to the advancement of aeronautics and space science. The NASA Scientific and Technical Information (STI) Program Office plays a key part in helping NASA maintain this important role.

The NASA STI Program Office is operated by Langley Research Center, the lead center for NASA's scientific and technical information. The NASA STI Program Office provides access to the NASA STI Database, the largest collection of aeronautical and space science STI in the world. The Program Office is also NASA's institutional mechanism for disseminating the results of its research and development activities. These results are published by NASA in the NASA STI Report Series, which includes the following report types:

- TECHNICAL PUBLICATION. Reports of completed research or a major significant phase of research that present the results of NASA programs and include extensive data or theoretical analysis. Includes compilations of significant scientific and technical data and information deemed to be of continuing reference value. NASA counterpart of peer-reviewed formal professional papers, but having less stringent limitations on manuscript length and extent of graphic presentations.

- TECHNICAL MEMORANDUM. Scientific and technical findings that are preliminary or of specialized interest, e.g., quick release reports, working papers, and bibliographies that contain minimal annotation. Does not contain extensive analysis.

- CONTRACTOR REPORT. Scientific and technical findings by NASA-sponsored contractors and grantees.

- CONFERENCE PUBLICATION. Collected papers from scientific and technical conferences, symposia, seminars, or other meetings sponsored or co-sponsored by NASA.

- SPECIAL PUBLICATION. Scientific, technical, or historical information from NASA programs, projects, and missions, often concerned with subjects having substantial public interest.

- TECHNICAL TRANSLATION. English-language translations of foreign scientific and technical material pertinent to NASA's mission.

Specialized services that complement the STI Program Office's diverse offerings include creating custom thesauri, building customized databases, organizing and publishing research results ... even providing videos.

For more information about the NASA STI Program Office, see the following:

- Access the NASA STI Program Home Page at ***http://www.sti.nasa.gov***

- E-mail your question via the Internet to help@sti.nasa.gov

- Fax your question to the NASA STI Help Desk at (301) 621-0134

- Phone the NASA STI Help Desk at (301) 621-0390

- Write to:
  NASA STI Help Desk
  NASA Center for AeroSpace Information
  7121 Standard Drive
  Hanover, MD 21076-1320

Available from:

NASA Center for AeroSpace Information (CASI)
7121 Standard Drive
Hanover, MD 21076-1320
(301) 621-0390

National Technical Information Service (NTIS)
5285 Port Royal Road
Springfield, VA 22161-2171
(703) 605-6000

Table of Contents

1. Abstract

The objective of this report is to contribute to the independent assessment of the Space Shuttle External Tank Foam Material. This report specifically addresses material modeling, characterization testing, data reduction methods, and data pedigree.

A brief description of the External Tank foam materials, locations, and standard failure modes is provided to develop suitable background information. A review of mechanics-based analysis methods from the open literature is used to provide an assessment of the state-of-the-art in material modeling of closed cell foams. Further, this report assesses the existing material property database and investigates sources of material property variability. The report presents identified deficiencies in testing methods and procedures, recommendations for additional testing as required, identification of near-term improvements that should be pursued, and long-term capabilities or enhancements that should be developed.

2. Introduction and Background

2.1. Space Shuttle External Tank

The Space Shuttle Transportation System (STS) in Figure 1 is composed of three major components: the orbiter, the external tank (ET), and the solid rocket boosters (SRBs). The orbiter and SRBs are attached to the ET. The ET provides fuel to the orbiter for the ascent phase of the STS since the orbiter only carries fuel for maneuvering while in orbit. The SRBs are attached to the ET and are used to lift the ET filled with fuel during the launch phase. When the ET has been drained of three fourths of the fuel, the SRBs are released (at approximately126 seconds). The orbiter and ET increase in speed and once escape velocity is reached at main engine cut-off (MECO) (at approximately 515 seconds), the ET is pressurized then released to burn up in the atmosphere during re-entry.

The ET has three major sections as shown in Figure 2; the liquid-oxygen (LO_2) tank, the intertank, and the liquid-hydrogen (LH_2) tank. The orbiter is attached to the ET at the top of the LH_2 tank with a bipod (a triangular strut) and at the bottom of the LH_2 tank with two longerons. The bipod and longerons are shown in Figure 2. The intertank is a cylindrical structure that connects with the LO_2 and LH_2 tanks. The SRBs are also attached to the ET through the intertank. The ET is coated with a spray-on cryogenic insulation that performs two major functions: to insulate to maintain propellant quality during fill and ground-hold, and to act as an ablative thermal protection system (TPS) during the ascent phase.

The polyisocyanurate cryogenic insulation NCFI-24-124 is sprayed on the acreage of the ET and is different from the polyurethane cryogenic insulation, BX-250 that is sprayed on the closeouts and areas not covered by the acreage cryogenic insulation [1]. Another closeout foam, BX-265 was used on other super-light weight (SLWT) external tanks, but not on the ET for STS-107. Locations of the acreage and closeout foams are shown in Figure 2. There are significant areas of the ET left bare during fabrication and assembly at the NASA Michoud Assembly Facility (MAF). Each major tank component (LO_2 tank, LH_2 tank, and intertank) is individually machine sprayed with NCFI-24-124, then assembled. A fair amount of the exposed areas, such as where the two propellant tanks are

mated to the intertank, bipod, longerons, feed lines and instrumentation ramp, are secondarily or manually sprayed with BX-250 or BX-265 at MAF or Kennedy Space Center (KSC).

After the failure of the Space Shuttle Columbia (STS-107) on February 1st, 2002, questions concerning the integrity of the cryogenic insulation on the ET of the Space Shuttle arose [2]. Debris from the ET was filmed falling off, then striking the left leading edge of the orbiter.

2.2. ET Foam Failure Modes

As reported by Knight et al., [3] the operating environment of the ET is a complex combination of thermal conditions, aerodynamic heating, aerodynamic and acoustic loads, and mechanical loads. Internally, the ET shell structure contains various amounts of cryogenic liquid fuels, while externally the ET is exposed to ambient air temperature and pressure prior to launch and aerodynamic heating and pressure, vibro-acoustic loading, and external pressure gradients during ascent. For weight savings, the structural capacity of the ET shell material is highly optimized. The structurally tailored shell walls of the LH_2 and LO_2 tanks are quite thin – in some regions the ratio of shell radius to shell thickness is much less than 0.001. As a result, the ET shell wall (substrate) deformations can be significant and may be a secondary contribution to many of the ET TPS failure modes.

The primary ET TPS failure modes appear to be a result of consequences stemming from the sprayed-on foam insulations (SOFI) application process and/or the overall ET system-level design. Detailed descriptions of the known failure modes for the ET SOFI system are presented in [3]. The failure modes include:

Substrate debond – This failure mode can result from poor adhesion of the SOFI to the ET aluminum substrate surface. Moreover, peel stresses caused by the thermal gradient and mismatch in thermal expansion between the substrate and the TPS, large-magnitude ET shell wall deflections (*i.e.,* hoop stretching of the cellular structure), and rapidly varying severe ET shell wall deflection gradients ("accordion mode") in the axial and/or hoop directions are major contributors to this failure mode.

- *Divoting* – This mode is a large-scale, cohesive failure mode that has been observed on several flights. This failure mode can result from entrapped gas within the foam cellular structure, cryoingestion of condensed liquid nitrogen from the intertank, and cryopumping of energy sources into local voids in the SOFI or substrate debonds near the substrate surface.
- *Popcorning* – This failure mode is a small-scale, cohesive failure mode that can result from small voids near the surface of the SOFI. In this case, if a vent path is absent or insufficient to relieve the gas pressure, a void located away from the substrate, in the through-the-thickness direction, that has entrapped gas in the foam cells causes a small popcorn-size piece of foam to "pop" off as the external pressure drops during ascent.
- *Delaminations* – This failure mode can result from SOFI disbond along the dense region between layers of the foam known as knit lines or from a coalescence of local failures of the SOFI cellular structure.

- *Transverse cracking* – This failure mode can result from local SOFI failures, substrate flexure, or from entrapped gas within the foam cellular structure. This mode can also serve as a relief mechanism for the delaminations, divots, and substrate debond wherein a transverse crack provides a leak or vent path for entrapped gas to escape.
- *Fragmentation/crushing* – This failure mode can result from external local impact of free-stream debris or ice that strikes the ET TPS and breaks off a SOFI fragment.
- *Strength failure* – This failure mode is essentially embodied in every failure mode and can result from external loading (discrete or distributed) that causes a material strength failure of the cellular foam system. This mode is singled out primarily to identify the strength-failure mode of the cell wall itself.
- *Aero-shear failure* – This failure mode can result from external aerodynamic loading caused by TPS protuberances in the flow field. Protuberances such as the bipod ramps, PAL ramps, ice/frost ramps, and feedlines are inherent to the vehicle and can result in a surface shear loading on the TPS. In addition, ET TPS surface roughness, manufacturing/processing variations, and small surface defects result in surface shear loading.
- *Fatigue* – This failure mode is related to the high-frequency loading caused by pulsating external loads. Flight conditions generate a time-varying high-frequency loading condition that can potentially contribute to a rapid flexing of the ET substrate. This flexing can cause fatigue of the bond between the foam and the ET substrate or cause local cellular fatigue failures that create voids. Another source of low-cycle fatigue that may precipitate failures is the propellant tanking/de-tanking process that often occurs prior to launch.

2.3. CAIB Report

The number one recommendation from the Columbia Accident Investigation Board (CAIB) report [2] was the elimination of debris shedding from the ET:

> R3.2-1 Initiate an aggressive program to eliminate all External Tank Thermal Protection System debris-shedding at the source with particular emphasis on the region where the bipod struts attach to the External Tank.

The findings of the CAIB indicated that a history of debris loss had occurred throughout the life of the Space Shuttle Program, even though the design requirements called for no debris loss during launch. All debris loss was ignored until STS-35 when foam shedding was called a “safety-of-flight issue” and “re-use or turn-around issue” but no significant action was taken. As missions continued, foam shedding became an “accepted risk” or “within experience base.”

Discounting foam debris ceased in 1999 when foam from the intertank region separated and struck the windward surface for STS-87. Over 308 strikes occurred, with 109 causing divots larger than 1 inch in length. An investigation followed and it was determined that a change in the blowing agent and the acreage spray material CPR-488 foam for the ET had precipitated this failure [2], [4]. The CFC-11 blowing agent was replaced with the HCFC-141b due to environmental restrictions and the acreage spray material was changed from

CPR-488 to NCFI-24-124. The findings of the investigation suggested that the new foam was stiffer than the older foam due to the blowing agent change, where the final rind (exterior sprayed surface) caused larger sections of foam to popcorn or shed from the ET during the ascent phase. MAF personnel reported that all of the popcorning occurred in the thrust panel region where the two SRBs connect to the ET intertank (Figure 1). In this region, the intertank is composed of external integrally machined aluminum blade stiffeners while the rest of the intertank is composed of external hat stiffeners. A number of measures were implemented to reduce the loss of foam during a launch. The exterior rind was machined off the intertank region. The machining process also reduced the thickness of the foam on the intertank to the minimum gage depth allowed based on the ablative properties of the foam. A minimum ablative gage was allowed because the intertank did not contain cryogenic fluids. The foam was also perforated and serrated with v-cuts to reduce the size of foam pieces that may potentially separate from the intertank. These measures reduced the amount foam debris on subsequent missions, but did not completely arrest debris from falling off during the ascent phase. The CAIB termed these fixes as ineffectual and concluded that the thermal-mechanical causes of the popcorning were never identified.

Loss of the foam from the bipod region occurred on six previous missions [2]. The bipod is shown in Figure 2 and is located at the top of the LH_2 ,above an internal ring frame. The number one recommendation from the CAIB report was the elimination of debris shedding from the ET.

3. Materials and Processes

3.1. Acreage Foam

Details on the chemistry, processing and application of ET foam materials can be found in the report by Weiser,et. al. [5]. For convenience, a brief description is provided herein. The three major components of the ET are covered with the NCFI 24-124 acreage foam [1]. This acreage foam is sprayed on the tank wall substrate with computer-controlled automated machines. There are areas shielded and left bare for the addition of secondary assembly parts. These bare areas are later covered with closeout foams.

3.1.1. Location

The LO_2 tank, LH_2 tank, and intertank are covered with the acreage foam. Figure 3 illustrates all of the areas where the acreage foam is used. The thickness of the foam can vary from 1 inch to 2 inches. Foam on the intertank is kept at a minimum thickness to reduce the amount of foam shedding due to popcorning. The thickness for the LO_2 and LH_2 tanks is based on the depth of insulation required to maintain propellant quality and quantity, and for ablative TPS during ascent. Intertank foam thickness is only based on the ablative depth required for ascent and continuity of the outer mold line (OML).

3.1.2. Previous and Current Formulations

Two types of acreage foams were used for the life of the ET. A history of the acreage foam usage is shown in Figure 4. The first 84 ETs used CPR-488 exclusively as the insulation foam material until ET-85, when the LH_2 tank was coated with NCFI 24-124.

CPR-488 was a polyisocyanurate material with a blowing agent of Freon-11 (CFC-11). The ET Project was forced to change from CPR-488 to NCFI 24-124 because of the loss of availability of components for producing the foam and the banning of the use of CFC-11. New foam, NCFI 24-124, with a blowing agent of HCFC-141b was introduced on ET-85 and phased in on subsequent ETs. Dates when the new NCFI 24-124 foam was introduced and on which ETs is in Figure 5. NCFI 24-124 is also a polyisocyanurate material.

3.1.3. Geometry, description

The foam is sprayed in layers of 3/8 inch in depth. A knit line separates each layer. These knit lines are also on a slight angle due to the rotisserie manner in which the tank is sprayed. A schematic of the foam is shown in Figure 6. A picture of the cell structure for BX-265 and a comparison to the morphology of other engineering materials is shown in Figure 7. This figure is provided to illustrate the relative size and complexity of the foam cell microstructure with respect to more typical engineering materials. The foam is light yellow in color after the initial application, and then darkens to a burnt orange color over time. Only the exposed top surface changes color. The exterior surface also has a rind layer that has an appearance similar to the rind of orange but courser. The exterior surface of the intertank is machined smooth.

3.1.4. Application and Process

An automated spray process was used to cover the acreage surfaces with the two-part foam [6]. Prior to the spraying process, all metallic surfaces were primed and cleaned. Non-metallic surfaces were coated and dried, and wires were coated with an epoxy primer.

Temperature and humidity of the work area and surface to be sprayed were measured and controlled. The parameters controlling the computer automated spray were the surface temperature of the part, ambient temperature, humidity, and atmospheric pressure. The foam density was monitored and expected to range from 2.0 to 2.5 pcf, and the target tensile strength was 30 psi. Table 1 contains the processing parameters for the acreage and closeout foams.

Each of the three tank components were each spun on a pedestal in a temperature controlled spray cell and sprayed. Three spray guns were mounted on an arm that moved up and down on a track. Multiple guns were employed because once the spray process began it could not be stopped. Each gun had a device that cleaned debris off of the end of the nozzle while spraying. When the internal pathways of the guns gummed with the foam, the next gun was used to spray the tank. The intertank spray cell has two arms, with each arm having three guns. Each of these guns was at an opposing angle to cover the complex exterior surface of the intertank. There was a minimal time-window allowed to spray over each layer. Overlap-time between courses or layers of foam was between 7 to 28 seconds. If the overlap-time was too long, the subsequent layer would not adhere to the previous layer. If the overlap-time was too short, the previous layer would not rise to the target thickness, and required cell size would not be achieved, and blowing agents would not have escaped. Also, if the subsequent layer was sprayed on too soon, there was the possibility of substantial heat build up that could possibly cause a fire hazard.

3.2. Closeout Foam

Closeout foams covered areas left bare, repair sites or test locations on the three major assembled tank components and secondary assembled parts. Various foams were used on the tank for different purposes. All of the closeout foams were polyurethane based foams. The closeout foams were manually sprayed on the surface and then after curing, manually sculpted to shape with knives.

3.2.1. Location

Most of the locations of the closeout foams on the ET are shown in Figure 3. Closeout foams were used to cover areas left bare after the acreage spray and final assembly for the ET such as the bolted-joint interface between the intertank and LO_2, and the intertank and LH_2 tank. The closeout foams were used to build up areas for secondarily added structures such as the bipod, longerons, feedlines, and instrumentation tray. Areas that were damaged due to handling or pull-plug testing were filled with closeout foams.

3.2.2. Previous and Current Formulations

A history of the closeout foam usage is shown in Figures 5. The foam known as BX-250 was the first closeout foam used on the ET. This foam was phased out due to the restriction of the CFC-11 blowing agent. However, a stockpile of CFC-11 was procured to continue using BX-250 into the year 2000. The foam SS-1171, with the blowing agent HCFC-141b, replaced a majority of the areas sprayed with BX-250, starting with ET-82. SS-1171 was discontinued by the year 2000. The ET project then reverted to using BX-250. A repair foam PDL-1034 has also been used throughout the life of the Space Shuttle Program. CFC-11 was also the blowing agent for PDL-1034, was but changed to HCFC-141b in 1995. The newest foam was BX-265, with the blowing agent HCFC-141b, and will replace BX-250 as the most used closeout foam. BX-265 was first introduced on ET-116.

3.2.3. Geometry, Description

The closeout foams were hand sprayed in layers, similar to the acreage foams. A knit line also separated each layer. The PDL-1034 was not used to fill large areas but was used to fill in holes left from plug pull tests, core samples, or repair at damage sites. The size of the closeout areas varied considerably. The maximum height of some the closeout sections is two to three feet.

3.2.4. Application and Process

A hand-spray process was used to cover the closeout areas with the two-part foam. Prior to the spraying process, all metallic surfaces were primed and cleaned. Non-metallic surfaces were coated and dried, and wires were coated with an epoxy primer. Two skilled technicians in environmental suits would manually hand spray the closeout foams in place.

Temperature and humidity of the work area and surfaces to be sprayed were measured and controlled. Other controlled parameters included the surface temperature of the part, ambient temperature, humidity, and atmospheric pressure. Table 1 contains the processing parameters for the closeout foams. The foam density was monitored and expected to range from 1.8 to 2.6 pcf. If more than one knit line was contained in the foam, the density could

be in the range of 1.8 to 3.0 pcf. A knit line is the dense region between foam layers as shown in Figure 6. The target tensile strength was 35 psi.

There was a minimal time-window allowed to spray over each layer. Overlap-time between courses or layers of foam was to be less than 45 seconds. Like for the acreage sprays, if overlap-time was too long, the subsequent layer would not adhere to the previous layer. If overlap-time was too short, the previous layer would not rise to the target thickness, the required cell size would not be achieved, and blowing agents would not have been able to escape. Also, if the subsequent layer was sprayed on too soon, there was the possibility of substantial heat build-up that could possibly cause a fire hazard.

If a cured foam layer was to be subsequently sprayed over with an additional layer of foam, the external rind was removed; the exposed layer was coated with a conathane adhesive and then sprayed according to STP 6014. After the closeout part has cured, the foam would be manually sculpted with knives to a specified shape.

4. Mechanics of Foam Materials

A suitable starting point for a review of the mechanics of foam materials is a summary of the models and methods provided by Gibson and Ashby in their book on cellular solids [7]. It is not the intent of this review to repeat all of the mechanics-of-materials relationships supplied in this text, rather to highlight some of the salient features as they apply to other works in the open literature. The reader is referred to Gibson and Ashby for a complete account of the derivation and use of the material relationships.

The nomenclature and approach provided in their book form the foundation of many of the mechanics models that have been published in the open literature. The basis for this nomenclature is the idealized unit cell illustrated in Figure 8. This figure defines the standard geometry of a closed foam cell and the reference coordinate system. Applying this unit cell geometry to the ET foam, Figure 6 illustrates the coordinate directions and features of typical sprayed-on foam. Using these figures, the following convention can be used:

Z_e	Number of edges that meet at a vertex (edge connectivity)
Z_f	Number of faces which meet at an edge (face connectivity)
$\overline{V}$	Number of vertices
$\overline{E}$	Number of edges
$\overline{F}$	Number of faces
$\overline{n}$	Mean number of edges per face
$\overline{f}$	Faces per cell
N_c	Number of cells per unit length (parallel to principal directions)

$\bar{L}_1$ Mean cell diameter $= \left(1.5 / N_c \right)$

ϕ Volume fraction of solid in edges

$(1-\phi)$ Volume fraction of solid in faces

ρ^* Foam density

ρ_s Base material density

$\bar{\rho}$ Relative density $= \left(\rho^* / \rho_s \right)$

$1 - \bar{\rho}$ Porosity

R Shape anisotropy ratio $= \left(h / l \right)$

Isotropic: R=1

Axisymmetric: single R value, Orthotropic: two R values

Depending on the temperature and the load levels, foam behavior can be elastomeric, elastic-plastic, or brittle. The transitions between linear elastic and nonlinear behavior also depend on the loading direction, foam-cell geometry, and other factors such as foam-cell internal gas pressure. In general, the following material properties can be used to fully characterize foam behavior:

ρ Density

E_i Modulus

G_{ij} Shear modulus

ν_{ij} Poisson's ratio

F_{iT} Tensile strength in *i – direction*

F_{iC} Compressive strength in *i – direction*

F_S Shear strength

K Stress intensity factor

σ_i Stress

ε_i Strain

The superscript $*$ is used with these symbols to identify the corresponding overall foam property. Similarly, the subscript s is used to indicate a base material property. The principal material directions are given by,

$$material\ directions \begin{cases} i = 1,2,3 \\ j = 1,2,3 \end{cases}$$

It is illustrative to provide schematic representations of the typical stress-strain behavior of a closed-cell foam, for the different types of behavior, under both tensile and compressive loads. These schematics are given in Figures 9 and 10. These figures depict the bulk behavior of the foam. Although the bulk behavior is, to a large extent determined by the behavior at the cellular level, the bulk response is of major interest due to the need for continuum-based mechanics models to predict deformation and failure. Prior to explanation of the schematics in Figures 9 and 10, it is worth considering material response at the cellular level that can influence measurements of bulk mechanical properties.

As noted in [7], the mechanical response of closed cell foam is highly dependent upon the relative amount of material concentrated in the cell edges and faces. In most cases, the majority of material is in the cell walls with a relatively thin cell wall membrane. Due to the nonuniform nature of the ET foam materials, it is necessary to assume average values of the cell geometric factors shown in Figure 8. The standard deviation of these factors can be considered to contribute to observed scatter in the experimental mechanical-property data.

During foam processing and application, the gases used as the blowing agent may become entrapped in the cell. The amount, pressure, and type of gas entrapped will affect the mechanical response of the cell and bulk material. This influence will be particularly evident during compression loading due to the ability of internal gas pressure to stabilize the cell and contribute to cell stiffness. Once again, the distribution of these gas-containing cells within the total bulk material will influence the degree of data scatter observed during mechanical testing.

Another factor to consider when examining measured mechanical behavior is the size effect that is typical of brittle materials. The assumption is that it is more probable that big specimens contain an inherent defect and will hence fail at lower stresses than a comparable small specimen. This effect of defects and scaling of properties, particularly properties sensitive to defects, must also be considered when examining measured properties.

For the ET foam materials, the existence of spray knit lines (Figure 6) and the anisotropic nature of the bulk material are also key factors related to the scatter of mechanical properties. The anisotropy arises from the rise of the material along the spray direction. Typically, closed-cell foams have the higher stiffness and strength in this rise direction. This geometry-dependent anisotropy is termed structural anisotropy as opposed to material anisotropy which is inherent in the base polymer material found in the cell walls. The anisotropy in the cell shape is given by the shape-anisotropy ratio, R, given above. Material properties, such as elastic moduli, strength, and fracture toughness can be found as a function of this shape ratio.

4.1. Tension

Referring back to Figure 9, the primary properties of interest during tensile loading are the elastic modulus and the stress level at transition. This transition is dependent on several factors and defined according to the type of behavior: cell-wall alignment (elastomeric), plastic yield (elastic-plastic), or fracture (brittle).

Based on a comparison to experimental data, the elastic constants could be represented using the following relationships

$$\frac{E^*}{E_s} \approx \phi^2 \left(\frac{\rho^*}{\rho_s} \right)^2 + (1-\phi)\frac{\rho^*}{\rho_s} + \frac{\rho_o (1-2\upsilon^*)}{E_s (1-\rho^*/\rho_s)} \tag{4.1}$$

$$\frac{G^*}{E_s} \approx \frac{3}{8}\left\{ \left(\frac{\rho^*}{\rho_s} \right)^2 + (1-\phi)\frac{\rho^*}{\rho_s} \right\} \tag{4.2}$$

$$\upsilon^* \approx \frac{1}{3} \tag{4.3}$$

where ρ_o is the initial gas pressure in the cell.

At strain levels beyond the initial elastic range, the response of the elastomeric material is governed by cell-edge bending followed by edge alignment and stretching (Figure 9a). This alignment can be visualized by considering the change in the angle between adjacent cell walls. The elastic-plastic behavior (Figure 9b) has a transition at yield due to plastic extension of the cell walls accompanied by cell wall alignment. For brittle foams (Figure 9c) facture will occur prior to cell wall alignment. For this failure mode, the use of linear-elastic fracture mechanics may be appropriate and the determination of foam fracture toughness is necessary to characterize the material. Assuming the foam behaves as a continuum, the singular stress field, as given by Gibson and Ashby [7], for a crack of length *2a* at a distance *r* from its tip is written as

$$\sigma = \frac{CK_1^*}{\sqrt{2\pi r}} \tag{4.4}$$

Where C is a constant related to specimen shape and K_1 is the stress intensity factor.

4.2. Compression

Throughout launch, the foam may be subjected to compression from aerothermal loading in selected areas of the tank. Referring to Figure 10, the initial response of foam in compression, regardless of response regime, is characterized by the elastic moduli. The small-strain linear-elastic modulus of foam for compression is the same as that for tension.

The mechanism associated with the transition from elastic to inelastic behavior depends on the material type. For an elastomeric material (Figure 10a), the stress-strain behavior may exhibit an extensive plateau region which is due to elastic collapse. Deformation in this region is recoverable upon load reversal. Beyond this plateau region, the cells undergo

rupture and behavior is characterized by densification of the foam. For cells with entrapped gas, compression of this gas will occur in this regime.

For an elastic-plastic material in compression (Figure 10b), the bulk material demonstrates a plastic collapse or plastic buckling when loaded beyond the elastic region. Deformation in this plateau region is not recoverable. The occurrence of this plastic collapse may be localized within the material, because as in the elastomeric material, further loading leads to densification of the material and an increase in apparent stiffness.

The transition in an elastic-plastic closed-cell foam material occurs when elastic behavior gives way to brittle crushing (Figure 10c). The crushing strength for closed-cell foams given by Gibson and Ashby [7] is

$$\frac{\sigma_{cr}^{*}}{\sigma_{fs}} = C_6\left(\phi\frac{\rho^{*}}{\rho_s}\right)^{3/2} + C_6^{"}\left(1-\phi\right)\frac{\rho^{*}}{\rho_s} \tag{4.5}$$

where σ_{fs} is the rupture stress of the cell-wall material, and C_6 and $C_6^{"}$ are material constants determined empirically.

4.3. Temperature, Strain Rate, and Environmental Effects

Closed-cell foams, such as those used on the ET, will exhibit both temperature and strain-rate dependence. The cell-wall material contributes to the inherent temperature and strain-rate dependence whereas the material properties of the entrapped gas contribute to the total temperature dependence of the material. In the elastic regime, Gibson and Ashby [7] give the approximation of modulus on temperature as

$$E_s = E_s^0\left(1-\alpha_m\frac{T}{T_g}\right) \tag{4.6}$$

Where E_s^0 is the modulus at 0 K, T_g is the glass transition temperature of the polymer, and α_m is a constant typically near a value of 0.5±0.2. For many polymers, elevated temperature, below glass transition, will lead to viscoelastic behavior and load-time dependent response characteristics such as creep and relaxation. Lower temperatures, approaching cryogenic, will increase the elastic regime but lead to lower strain-to-failure values than compared to room-temperature values.

Strain-rate dependence is most apparent beyond the elastic region with yield stress and strength increasing with an increase in strain rate. The degree of strain-rate dependence is highly dependent on temperature, material type, and foam-cell geometry. Dynamic events, such as high-speed impact, are associated with high strain-rate effects. Often, these dynamic events have strain rates that are at least four orders of magnitude higher than events associated with non-impact loading.

Few investigators have published experimental data on environmental effects on closed-cell-foam behavior to date. In a recent report, Li and Wietsman [8] presented results from long-term sea-water exposure tests of polyvinyl chloride (PVC) foam materials. Their data showed that after immersion in sea-water, for periods up to two years, the majority of the water absorption was confined to the exterior regions and would reach saturation within

two months. Absorption in the crack-tip regions of fracture specimens increased the toughness of the foam and decreased the debonding fracture toughness at the core-substrate interface. The finite element method was used to predict the fracture behavior and was validated with experimental data.

4.4. Size and Scaling Effects

To develop finite element models that describe the bulk thermal-mechanical behavior of the ET foam, it is desirable to consider the foam as a continuum material. However, the ET foam material has several inherent geometric or size scales that must be considered when formulating analysis models and test methods for material properties.

The base polymer material is considered to be at the lowest part of the size scale, with properties that may be anisotropic due to orientation effects that occur during processing. At the next larger scale, a typical foam cell has geometric features that are amenable to a micro-mechanics approach. As typical with this approach, the definition of the material relies upon a unit cell and a representative volume element. Further homogenization of the material system leads to the description of the foam as a continuum with a set of averaged properties. Although it is advantageous to consider the continuum material, one possible difficulty is associated with the scaling of defects that lead to bulk material failure.

This scaling problem was addressed by Brezny and Green [9] for a brittle reticulated vitreous carbon foam. In this study, the elastic modulus, fracture toughness, compressive strength and bending strength were measured as a function of cell size and analyzed by using a micromechanical model. Results indicated that the elastic modulus and fracture toughness showed no cell size dependence. It was noted that the variation in cell strut strength as a function of cell size had to be accounted for to ensure the model accurately predicted toughness. It was also found that compressive strength increases inversely with cell size.

An investigation of structure size on the strength of closed-cell PVC foam was investigated by Bazant et. al. [10]. This study considered two types of size effects – Type I, characterizing failure of structures with large cracks or notches, and Type II, characterizing failure at crack initiation. Tensile mode I fracture was experimentally determined for a range of specimen widths while holding the length-to-width ratio constant at 5:2. Notches were cut to a depth of 0.4 times the width which ensured failure to occur at the notch location, avoiding the influence of the standard distribution of defects. Loading was performed at a constant displacement rate. The fracture was considered brittle and behavior was nearly that as predicted by linear elastic facture mechanics. Fracture toughness, as a function of geometry variations, was given as

$$K_c = \sqrt{E' G_r} \tag{4.7}$$

Where E' is Young's modulus (plane stress) and G_r is the fracture energy determined from tests. Type II tests included a rectangular specimen, loaded in tension, with center holes of varying diameter-to-width ratios. The general conclusion from all of the results was that the influence of size is important and must be taken into account for cases such as those that occur when large damage zones appear prior to critical loading to failure in large structural parts.

4.5. Core-substrate Debond

One important failure mode of the ET foam material system is initiation and growth of a debond between the foam and the metal substrate. In a paper by Viana and Carlsson [11] it was assumed that the intrinsic fracture toughness of the foam would strongly influence the debond toughness between the foam and the substrate. The results, experimental in nature, were based on the debond fracture toughness of a foam core sandwich with composite and aluminum facesheets. The foam was a PVC material and several foam densities were tested. Debond fracture toughness was found from tests as a function of critical strain energy release rate and the compliance calibration method. In general it was found that the debond fracture toughness increased with increasing core density and did not depend on substrate or facesheet material.

In another report by Viana and Carlsson [12], on the same PVC foam material, both the tensile stress-strain behavior and the fracture response were measured as a function of foam density. It was found that the expressions given in Gibson and Ashby [7] correctly described the scaling of the modulus and the yield strength as a function of foam density. The fracture toughness followed a linear relation in density and the toughness decreased with decreasing specimen size.

4.6. Multi-axial Loading, Failure

Failure of closed cell foams was investigated experimentally by Gdoutos, et. al. [13],[14]. In this study, they obtained the uniaxial tensile, compressive and shear stress-strain curves along the in-plane and through-the-thickness directions as well as biaxial data using specialized specimen geometries. The data was compared to the theoretical Tsai-Wu failure criteria [15]:

$$f_1\sigma_1 + f_3\sigma_3 + f_{11}\sigma_1^2 + f_{33}\sigma_3^2 + 2f_{13}\sigma_1\sigma_3 = 1 - k^2 \tag{4.8}$$

where

$$\begin{aligned} &f_1 = \frac{1}{F_{1t}} - \frac{1}{F_{1c}},\ \ f_3 = \frac{1}{F_{3t}} - \frac{1}{F_{3c}},\ \ f_{11} = \frac{1}{F_{1t}F_{1c}},\ \ f_{33} = \frac{1}{F_{3t}F_{3c}} \\ &f_{13} = -\frac{1}{2}\left(f_{11}f_{33}\right)^{1/2},\ \ \tau_5 = kF_5 \end{aligned} \tag{4.9}$$

In these equations, $\sigma_1, \sigma_3, and\ \tau_5$ are the normal and shear stress components referred to the principal material directions (Figure 8), k is a constant, and F_{ij} are the strength parameters along a material direction for tension and compression.

From the test data, it was determined that the elongation of the cells along the rise direction resulted in material anisotropy with the stiffness and strength in the rise direction exceeding the values for the in-plane directions. Other key results included: Poisson's ratio in the yield region, while under compression, approached zero, and the biaxial tests exhibited similar characteristic features and material response of the corresponding uniaxial tests. The failure surfaces from combined load tests were predicted by the Tsai-Wu failure criterion.

In a study of failure of isotropic foams, Christensen et.al. [16] considered the development of failure criteria considering both yielding (ductile materials) and fracture (brittle materials). For low-density foams, the proposed polynomial failure criteria was given as:

$$\left(\frac{1}{\tilde{\sigma}_{11}^{T}}-\frac{1}{\left|\sigma_{11}^{C}\right|}\right)\sigma_{ij}+\left[\frac{1}{\tilde{\sigma}_{11}^{T}\left|\sigma_{11}^{C}\right|}-\frac{1}{2\left(\sigma_{12}^{Y}\right)^{2}}\right]\sigma_{ij}^{2}+\frac{\sigma_{ij}\sigma_{ij}}{2\left(\sigma_{12}^{Y}\right)^{2}}\le 1 \qquad (4.10)$$

where σ_{ij} are the principal stresses at failure, the failure directions are in tension (T) and compression (C) and shear (Y), and $\tilde{\sigma}_{11}^{T}$ is the tensile strength that would exist if there were no brittle-facture cutoff. It is noted that the brittle facture value could be less than or greater than $\tilde{\sigma}_{11}^{T}$ and the shape of the failure surface would be modified accordingly. It is also noted that for many low-density foam materials, $\left|\sigma_{11}^{C}\right|\le\tilde{\sigma}_{11}^{T}$ but is not necessary for implementation of the failure criteria. Experimental data was compared to the predicted failure surface and agreement between test and prediction was facilitated by using the tensile strength cutoff due to brittle fracture.

In another study, Benderly and Putter [17], investigated the shear/compression failure envelope of a PVC foam using both experimental data and finite element modeling. A modified four-point flexure test was proposed to measure shear strength. The failure envelop for the combined compression/shear loading was found for a range of loading conditions and at three temperatures (-40^{o}C, RT, +70^{o}C). In all cases, the failure envelope was adequately represented by the fit of an ellipse to the data.

An elliptic-paraboloid failure surface was utilized by Theocaris [18] in the study of failure in closed-cell polyurethane foams. Experimentally, samples were tested in simple tension and compression along the three principal material axes. It was found that the material could be adequately represented as transversely isotropic material. Due to the significant differences between elastic buckling in compression and brittle facture in tension, the proposed failure surface was best represented by the intersection of an ellipsoid and the elliptic-paraboloid surface. The failure surface was described as

$$H_{11}\sigma_1^2+H_{33}\sigma_3^2+2H_{31}\sigma_3\sigma_1+h_1\sigma_1+h_3\sigma_3=1 \qquad (4.11)$$

Where $(\sigma_1,\sigma_2,\sigma_3)$ are the principal stresses and *H*, and *h* are terms from the failure tensors that are defined in terms or the basic strength properties of the material.

4.6.1. Notch, Defect Sensitivity

The foam materials on the ET are prone to defects and voids due to the application process and the variable geometry of the substrate. The presence of these defects must be considered by accounting for scatter in the test data and the applicability of fracture or strength analysis.

For a standard Wiebull distribution of defects [19], the probability of fracture at a load *z* is given by

$$\xi(z) = 1 - \exp\left[-\left(\frac{z - z_o}{z_a}\right)^{\beta}\right] \tag{4.12}$$

where z_o, z_a, and β are the location, scale and shape parameter, respectively.

In a general study of defects in engineering materials, Todinov [20] presented equations related to spatial statistics of defects and the probability of detecting defects in one-dimensional components. The equations related to spatial statistics of defects allow one to estimate the probability of existence of safe, defect-free zones between the defects in one-dimensional components. The proposed probability of fracture was

$$S(\sigma) = 1 - \exp\left[L\sum_{i=1}^{M}\mu_i \ln\left(1 - pF_i(\sigma)\right)\right] \tag{4.13}$$

where $\mu = n/L$ is the number density of the defects calculated on the basis of the calibration length L, n is the number of defects in the calibration length and $p = \Delta L/L$ is the ratio of the stressed length ΔL to the entire calibration length L. The function $F(\sigma)$ is a cumulative probability of triggering fracture associated with the defects, i.e. the probability that a randomly chosen defect from the population will trigger fracture at a stress smaller than or equal to σ. The length L was referred to as 'calibration length', necessary to determine the defect number density μ.

It was demonstrated by Todinov that even for moderate defect densities, the probability of existence of clusters of two or more defects at a critically small distance is substantial and should not be neglected in calculations related to risks of failure. It was demonstrated for large tested fractions from one-dimensional components, the failures are almost entirely caused by a small part of the largest defects, whereas, for small tested fractions, almost all defects participate as initiators of failure.

In a study of metallic foams, Paul et al. [21] experimentally investigated the notch sensitivity under simple tension loading. It was found that the material was insensitive to notches that had the notch root diameter smaller than the characteristic cell diameter. For notch root diameters that exceeded this cell diameter, the net strength decreased as notch root or hole diameter increased.

Both experimental and analytical (finite element) studies of the effect of stress singularities on the strength of PVC foam, at room temperature, was made by Grenestedt et al. [22]. Using materials with different densities, the study focused on the specimens with different wedge geometries ranging from sharp cracks to shallow reentrant corners. For the sharp cracks, good agreement was found between test and the calculated critical stress intensity factor based on brittle fracture criteria. It was found that, in general, the failure loads of specimens with sharp cracks were less than half of the failure loads of specimens with smooth cut-outs. Further, it was concluded that the same criteria as used for homogeneous material could be used for the foam materials. The parameters for the proposed failure criterion could be found from two tests, one un-notched specimen and one sharp crack specimen.

Andrews and Gibson [23] examined notch strengthening under tensile load; the net section strength of a crack section being greater than the tensile strength of the intact foam. The cases examined were for open-cell aluminum foam with a nominal cell size of 40 pores per inch. Based on the experimental data, it was postulated that failure, at the cell level, was due to tensile failure of the intact cell ligament combined with localized shearing at the crack tip.

In another study on metallic foams, Olurin et al. [24] measured the compressive, tensile, and fracture behavior of closed-cell foams with selected densities. Notch sensitivity was measured using a double-edged notch specimen and fracture toughness was determined using a standard compact tension specimen. It was found that the yield strength, unloading modulus and toughness increased with the relative density of the foam. The notched tests revealed a small degree of notch strengthening, however the strength properties are generally notch-insensitive. A significant R-curve behavior was observed in the fracture tests and was attributed to cell edges bridging the crack behind the observed crack tip.

4.6.2. Fracture Toughness

Fracture toughness of foam is often measured with a notched beam loaded in three or four-point bending. As presented by Smith [25], the Model I fracture toughness is given by

$$K_I = \frac{4P_f\sqrt{\pi}}{Bw^{1/2}}\left(1.6\left(\frac{a}{w}\right)^{1/2} - 2.6\left(\frac{a}{w}\right)^{3/2} + 12.3\left(\frac{a}{w}\right)^{5/2} - 21.2\left(\frac{a}{w}\right)^{7/2} + 21.8\left(\frac{a}{w}\right)^{9/2}\right) \tag{4.14}$$

where a is the crack length, w is the beam width in the direction of the crack, B is the beam thickness, and P_f is the fracture load. In Gisbon and Ashby [7], the relationship of foam fracture toughness to foam density is given by

$$K_{Ic} = c\sigma_\infty\sqrt{\pi a}\left(\frac{\rho^*}{\rho_s}\right)^{3/2} \tag{4.15}$$

where c is a material constant, σ_∞ is the far-field stress and the density expressions were defined previously.

The Mode I fracture toughness of open-celled carbon foam was measured by Choi and Sankar [26] using a single-edge notched, four-point bending specimen. The crack tip region was modeled using finite elements and micromechanics models were developed assuming a rectangular prism as the unit cell and orthotropic material properties. The Mode I fracture toughness was calculated from the experimentally measured load at failure using

$$K_I = \sigma_\infty\sqrt{\pi a}\left(1.12 - 1.39\frac{a}{w} + 7.3\frac{a^2}{w^3} - 13\frac{a^3}{w^3} + 14\frac{a^4}{w^4}\right) \tag{4.16}$$

where σ_∞ is the maximum bending stress in the uncracked beam, a is the crack length, and w is the width in the direction of the crack. The stress intensity factor was determined from the finite element model and was used to predict the fracture toughness of the foam.

Through the use of solid finite elements to model the foam, good agreement was reached between the measured and predicted fracture toughness.

4.6.3. Fracture Behavior of ET Foam

Based on the work of Jerman [27], typical fracture features of the BX-265 material were dependent upon test temperature. At room temperature, observation of the failed cellular structure included random cell edge fracture points, plastically deformed fractured cell walls and fractured cell walls reoriented perpendicular to the fracture plane. At cryogenic temperature, these same features were observed, however, some of the cell fracture behavior appeared brittle in nature – cell edges appeared mostly intact instead of random. For the ET application, the facture behavior of the foam is complicated by temperature gradients in the foam and the possible occurrence of combined damage mechanisms such as cryopumping and void formation.

In a related, undocumented NASA-Marshall Space Flight Center (MSFC) briefing, dated March 19, 2004, the status of fracture test data and sample interface K solutions were summarized. Test data to date indicated that application of the stress intensify factor using the isotropic homogeneous material assumptions are valid as long as all length scales for the cracked specimen (crack length, ligament, thickness, etc.) are very large compared to the cellular microstructure.

The BX265 foam behaves in a predominantly brittle fashion, reducing or eliminating constraint effect of observed toughness. This behavior should permit a single parameter (K) approach to predicting failure in foam with sharp or crack-like defects.

In-plane fracture properties appear equivalent within the expected variability of the material. All rise-direction toughness values are significantly higher than the corresponding in-plane values. Cryogenic toughness for in-plane orientations is lower than room temperature values. Cryogenic toughness for rise direction is roughly equivalent to the room temperature value.

5. Test Methods and Characterization

Test plans were developed and implemented to determine mechanical properties and for the purpose of material qualification. The existing databases include data from tests that characterize the material. A summary of the tests performed for material characterization and qualification is listed in Table 2. Descriptions of the tests are also provided in this section. The tests outlined in this section are taken from the descriptions provided by [2]. Each test is briefly described and referenced to the appropriate test standard.

5.1. Mechanical Property Tests

The mechanical property tests are performed at temperature ranging from -423°F to 350°F. The tests are

Plug pull testing is a tensile test that is performed 24 to 72 hours after test panels are sprayed. Plug pulls are taken at room temperature with standard TPS Bond Tension Tester equipment according to OP-13M50-FT and OP-13M51-FT. Panels are machined to a thickness of one-inch above the substrate and a coring tool is used to

extract a one-inch diameter specimen from the panel. Test results indicate the flat-wise tensile strength of the material in the rise direction. The data from these tests is primarily used as a quality assurance check and will not provide tensile data that may be required for constitutive model development.

Lap shear tests are performed at room temperature and elevated temperature in accordance with TTP-2007. Test results provide a range of values for shear strength. These tests do not provide data at cryogenic temperature, shear stress-strain behavior or information on the influence of material anisotropy.

Flexure test specimens are tested in accordance with test procedure TTP-2006. Flexure specimens in a four-point bend configuration are tested to failure at room temperature. Outer fiber strain is calculated. This test investigates a beam or structural response. The data from these tests is primarily used as a quality assurance check and will not provide material properties required for modeling or validation.

Bond tension tests are performed at cryogenic, room and elevated temperature in accordance with ASTM D1623. Test specimens are two-inch square samples adhered to a metal substrate and two metal loading blocks. Test results provide an indication of bond-to-substrate integrity although the load on the bondline is not representative of typical loads generated during flight.

Monostrain testing is performed at cryogenic, room temperature and elevated temperatures in accordance with TTP-2002. The standard specimen is suspended between two clevises and tested to failure. The results of testing determine the derived properties of thermal strain, ultimate tension, strain at failure, and Young's modulus. The influence of material density changes and anisotropy will only be evident if the test specimens are cut along principal material axis and within regions of uniform density.

Gradient cryoflex tests are performed in accordance with EQTP 1002. Cryoflex specimens are fabricated on Al-2195 substrate using selected spray conditions. All other specimens are fabricated on Al-2219 substrate. Testing takes place at a substrate temperature of -320°F and -423°F while the foam face of the specimen remains close to room temperature. Specimens are tested to failure or to the limits of the test fixture. At the small-scale or coupon-level, the cryoflex tests provide the best representation of external tank variable temperature conditions. The results quantify the defect tolerance vicinity of the TPS/substrate bondline interface under simulated service conditions.

Compression and density are accomplished using the same specimen at room temperature according to LI P-004 and LI P-006, using standard 2 by 2 by 3/4 - inch blocks of BX-265. Specimens are measured and weighed to determine density, then tested for compression. Allowable compression is based on 10% deflection.

Poisson's ratio is determined at room temperature in accordance with TTP-2003. The material is subjected to a compressive force, and the specimen is monitored for strain, change in diameter, and change in length.

5.2. Thermal Property Tests

Thermal property testing is done to verify that the process environment would not affect the thermal properties. The thermal property tests are

Thermal-vacuum testing is performed at four heating rates (2, 4, 6, and 8 btu's). Thickness and weight measurements are taken on each test article before and after the testing. This test simulates the foam surface-heat loading and atmospheric pressure on the external tank during flight. The thermal-vacuum testing determines the materials performance in a radiant heating environment, and failure modes seen on the intertank thrust panel can be produced.

Hot gas panel testing is performed at the Hot Gas Facility (HGF) at Marshall Space Flight Center. The test is performed at three heating rates (4, 8, and 12 btu's) in accordance with HGF-TCP 001. Thickness and weight measurements are taken on each test article before and after the testing. The hot gas panel test is designed to assess the materials recession performance in an assent environment.

Thermal conductivity testing is performed at cryogenic, elevated, and room temperatures in accordance with ASTM C177. The test results are used to determine the thermal conductivity of the material.

Specific heat is determined in accordance with ASTM E1269. The temperature range is determined by the testing method chosen, either Holometrix quantitative thermal analyse (QTA) or Seiko differential scanning calorimetry (DSC).

5.3. Receiving Acceptance Tests

Acceptance criteria and fingerprinting tests are performed to verify the formula consistency from batch to batch. Receiving and acceptance tests are performed upon receiving, and three months, six months, nine months, and twelve months later. The acceptance tests are

Viscosity of both A and B components of the two-part foam are performed according to STM L742/STML1B3.

Specific gravity of both A and B components of the two-part foam are tested for specific gravity according to STM L742/STML1B3.

Amine equivalent of component A is determined according to STM L742/STML1B3. This test measures the reactive isocyanate present in the material.

Moisture content of component B is determined according to STM L742/STML1B3

Hydroxyl number of component B is determined according to STM L742/STML1B3. This test measures the reactive hydroxyl groups present in the material.

Acid number test is performed according to ASTM 4662.

Reactivity of the foam material is determined according to STM L742/STML1B3. The specified portions of components A and B are mixed for a period of time, then the times for cream, rise, tack-free recorded.

5.4. Fingerprint Tests

The objective of the fingerprint tests is to determine the consistency and quality of the TPS systems. The fingerprint tests are

Gas chromatography with thermal conductivity detector is performed on the B component of the two-part foam in accordance EQTP 1003K, LI G-024. This test determines the concentration of the blowing agent present in the material.

Gas chromatography with flame ionization detector is performed on the B component of the two-part foam in accordance EQTP 1003K, LI G-019/G-074. This test determines the concentration of other volatile ingredients present the material.

Inductively coupled plasma atomic emission spectroscopy is performed on the B component of the two-part foam in accordance EQTP 1003K, LI S-103 and S-110. This test determines the concentrations of elements related to the surfactant.

Fourier transform infrared spectroscopy (FTIR) is performed on the B component of the two-part foam in accordance with paragraphs 4.1 through 4.5 of LI S-107/S-136. Testing determines the functional groups related to composition and relative amounts of polyols, flame-retardants, and blowing agent present in the material.

Gas chromatography/nitrogen-phosphorus detection testing is performed in accordance with EQTP 1003K, LI G-046. Testing determines the amount of amine catalyst present in the material.

5.5. Environmental Effects Study

An environmental effect study included the 180-Day PAD study that assessed the TPS property changes due to climate exposure characteristics of one season. The intent of this study was to determine if exposure to the natural environment at KSC would degrade the TPS material properties that would compromise the mission. Property changes that were considered included thermal conductivity, bond tension, cryoflexure, dimensional change, weight change, and substrate inspection.

A Six-Year-Storage Study is also planned that will evaluate the cryogenic strain compatibility, corrosion and aging effects of TPS materials on primed aluminum alloys. Test panels will be prepared with appropriate primer/TPS materials and evaluated for cryogenic strain compatibility (cryoflex and bond tension), corrosion (accelerated corrosion testing) and aging (cryoflex, bond tension, primer adhesion and corrosion inspection annually for up to six years) effects.

Aging of polymeric materials can include both physical aging and chemical aging mechanisms. Physical aging, associated with gradual evolution of the polymer to thermodynamic equilibrium, is ubiquitous and can be quantified by controlled series of time-dependent tests such as creep or stress relaxation. Elevated temperature (sub Tg) can be used to accelerate the physical aging. Chemical aging, associated with process such as polymerization, polymer chain scission or changes in crosslink density can be quantified by controlled thermal analysis such as dynamic mechanical analysis, thermal mechanical analysis or differentiating scanning calorimeter. Elevated temperature (sub Tg), moisture, and oxygen can accelerate chemical aging. Mechanical properties will be affected by both types of aging however the difficulty in measuring static mechanical properties as a

function of aging time makes mechanical testing a less desirable means for aging assessments.

6. Materials Database

The tests results for the material properties of NCFI 124-24 for the LO_2 tank and barrel section, BX-250, and BX-265 were provided by MAF. The requirements for density and tensile strength placed on the ET Project are listed in Table 1.

A portion of the data sets contained only the maximum (high), mean (average) minimum (low) and standard deviation. The data was also listed in data sets by lots and test temperature conditions. Test temperature conditions were -423°F, -320°F, room temperature (RT, +75°F), +100°F, +200°F, +300°F, and +350°F. MSFC and MAF personnel managed the databases. The material data bases were tracked by the components used, spray conditions, and date the foam was sprayed.

6.1. Results

A portion of the data from the test listed in Table 2 is shown in Tables 3-7. The data in these tables were for the acreage foam NFCI-24-124, the closeout foam BX-250, and the closeout foam BX-265. The results of the flatwise tension and bond tension for NFCI-24-124 are plotted in Figures 11 and 12. The results for the flatwise tension tests and Young's modulus for BX-265 are plotted in Figures 13 and 14. For both these data sets, considerable scatter exists at each temperature making it difficult to assess trends. However, the general trend in flatwise tension strength indicates that the elevated test temperature (200°F) has the lowest strength. Similarly, the tensile Young's modulus data has the lowest values at the 200°F test temperature.

In Tables 6 and 7, data from results for derived monostrain ($\alpha\Delta T$, ultimate strain, failure stress, and Young's modulus), flatwise tension, bondline tension, compression, and density tests are listed. These tests were performed at various temperatures (-423°F, -320°F, RT [+75°F], 100°F, +200°F, +300°F, +350°F). Not all of the tests were performed at every temperature. There were results at RT for almost all of the tests. Whether or not a plot was made for a test was based on available individual test data points for that test. Plots of the results in Figures 11-14 were made for tests that had high, average, low values, and standard deviation with individual test data points.

6.1.1. Acreage Foams

The results for the acreage foam NFCI-24-124 for the LO_2-tank ogive and barrel section are listed in Tables 3 and 4. There was no derived monostrain data reported, thus, a large portion of the data in the tables is missing. Tables 3 and 4 contain the bond tension, flatwise tension, RT compression, and RT density test results.

The results for the ogive NFCI-24-124 foam in Table 3 indicates that the average density, 1.91 pcf, is lower than the required value in Tables 1 of 2.36 pcf. The average bondline and flatwise tension strengths are all greater than the required 30 psi listed in Table 1, except for the results for +300°F. These results are 28.4 psi and 26.4 psi for

bondline and flatwise tension strength, respectively. Test results where the high and low values exceeded the +/- 2 Sigma of the test data are indicated in Table 4 in red and **bold**.

The results in Table 4 indicate that the average density, 2.26 pcf, is close to the average required density of 2.25 pcf. The average bond tension and flatwise tension strengths are all above the required tensile strength of 30 psi in Table 1. However, the standard deviation of these results is high and all of the low bond tension and flatwise tension strength results are below the required values. The results listed in Table 4 indicate that the data for the bond tension and flatwise tension tests for all temperatures, have a large amount of scatter even though a large number of replicates was used. The results for RT compression and density did not have as much scatter as the other two reported test results. Test results where the high and low values exceeded the +/- 2 Sigma of the test data are indicated in Table 4 in red and **bold**. The plots in Figures 11 and 12 show how wide spread the scatter is for the data at various test temperatures. The data in Table 4 was also reported by lots and is listed in Table 5. Even though the data was separated by lots, there was no clear bias for better results from either Lot 2 or Lot 3. Lot 3 had higher values for bond and flatwise tension strengths compared to Lot 2, but the results for compression and density were lower. Lot 3 also had a lower standard deviation in strength than Lot 2.

6.1.2. Closeout Foams

The results for BX-250 are listed in Table 6. There are no standard deviation numbers listed and the individual data points were not available since this was an Apollo-Program-era foam. There was no flatwise tension strength data to compare to the 35 psi requirement listed in Table 1. The average density of 2.15 pcf is close to the required 2.2 pcf average density for BX-250 with only one knitline. The average density number in Table 6 is far below the required 2.4 pcf average density if multiple knitlines exist.

The results in Table 6 indicate that this foam tends to expand as the temperature decreases. The results in Table 6 also indicate a large amount of scatter in the data since the high and low values are very different than the average. Unfortunately, the standard deviation and the individual data results were not provided. All of the results in Table 6, for all of the temperatures, follow the same trend in which the high and low values are very different than the corresponding average value.

The results for BX-265 are listed in Table 7, and the corresponding results for the flatwise tension strength and Young's modulus are plotted in Figures 13 and 14. The flatwise tension strengths are above the required 35 psi for all temperatures. The lowest flatwise tension strength values are also above the corresponding –2 Sigma values. There is a large amount of scatter in the results for the flatwise tension strength data. The bond tension strength data is also above the required 35 psi for all temperatures.

The reported average density of 2.38 pcf for BX-265 exceeds the required 2.20 pcf average density for material having only one knitline. However, the reported density of 2.38 pcf is very close to the required 2.4 pcf average density for multiple knitlines. The remaining results listed in Table 7 indicate that all of the results, for all temperatures, have a large amount of scatter even though a large number of replicate tests were used. Test results where the high and low values exceeded the +/- 2 Sigma of the test data are indicated in Table 7 in red and **bold**. The plots in Figures 13 and 14 show how wide spread the data is for the various temperatures.

6.2. Material Processing and Constituents Review

The data generated from the testing of the ET foams exhibits a large degree of scatter. The scatter is depicted in Figures 11, 12, 13, and 14 for the flatwise and bondline tension tests of the NCFI 24-124 acreage foam and the flatwise tension and Young's modulus tests of the BX-265 closeout foam. Almost the entire scatter was contained within the +/- 2 Sigma bounds but there is uncertainty concerning the quality of the data. The uncertainty pertains to the true acceptable lower allowable value, the extent of the testing, and the lot-to-lot material variability.

A portion of the data was separated by lots, but most of the provided data was listed as a total data set for one lot of material. If the data had been separated by lots, the data would have been helpful to determine if the processing parameters played a significant role. Reports from other teams have determined that there was a great deal of variability in the raw materials, processing parameters, and processing methods. The following excerpts were taken from reference [5].

> "A major change that occurred in the late 1990's was the use of a new blowing agent, HCFC 141b. The CFC 11 blowing agent had been standard as far back as the Saturn V [rocket for the Apollo Program]. This material was known to be an ozone-depleting substance and the entire foam insulation market was transitioning over to HCFC 141b. NASA was forced to follow this trend because the CFC 11 was disappearing from the commercial market. This change in blowing agents was a major change since the HCFC 141b had a higher boiling point that required a higher application temperature for the ET foam. This higher application temperature carried with it a higher reaction rate for the foam formation. Also, the chemical structure of HCFC 141b has an appreciably larger dipole that most certainly results in more solubility of the blowing agent in the foam cellular walls.
>
> ….this study, [a comprehensive Thermogravimetric Analysis/Mass Spectrometry (TGA-MS) tests], will be done [at LaRC] in order to verify preliminary data related to the evolution of blowing agent; to study the volatiles associated with a continuation of the chemical reactions of the residual raw materials; and to study the decomposition by-products as the foams are exposed to temperatures that approach their stability limits.
>
> A serious concern is that the lower limit for spraying the BX-265 (with the higher boiling HCFC 141b) is 70°F, a temperature well below the boiling point of the blowing agent. The boiling point of HCFC 141b is 90°F. This could result in inadequate blowing of the foam and in having an excessive amount of entrapped blowing agent well below the surface of the foam. In the case of BX-250, the boiling point of CFC 11 is 70°F and the lower spray temperature is 65°F. It is strongly suggested that this lower temperature limit for BX-265 blowing be re-examined. Failure to do so could result in void formations ….
>
> The need for more chemical structural knowledge is important for all of the components in the foams. An expansion of this area is recommended for the Analytical Lab at MAF. This will involve learning about, documenting, analyzing and tracking all components on a routine basis. This expanded knowledge of the raw material chemistry along with TGA-MS data studies on the final foams will allow the MAF Analytical Lab to operate in the same manner that their counterparts in the commercial manufacturing sector operate today. Analytical Chemistry is a rapidly changing science that is a very powerful tool in the quality manufacture of any material."

From these excerpts, the significant problems can be seen and possible solutions can be inferred. For example, a change in the blowing agent required an increase in the lower limit of the spray temperature from 65°F to 85°F. If the blowing agent was not completely vaporized during the spraying process, an excessive amount of blowing agent could be

entrained in the final cured foam. The HCFC 141b blowing agent was also much more soluble than the discontinued CFC-11 blowing agent. Using thermogravimetric analysis/mass spectrometry (TGA-MS) tests, it was determined that volatiles such as HCFC 141b were still being expelled from the cured foam. These entrained volatiles could cause voids to be formed in the foam as the foam heated during the cure process (the foam heated internally as it cured and was insulated with each subsequent layer being added) and foam to separate or burst during the ascent phase due to aerothermal heating. The TGA-MS could also be used to fingerprint and verify the make-up of the raw materials before being used and after the foam has cured in the laboratory. Fingerprinting could also be used on the production floor to ensure that the same material fabricated in the laboratory is the same material being placed on the ET.

The chemical processing and materials report presented by Weiser, et. al. also documented that the materials used in the ET foams are a low production item or low priority item for the vendors that supply these materials. NASA is subject to changes or discontinuation of ingredients without notice or the ability to request similar formulations of the original materials. An example that was cited was the change in a catalyst from organotin 125 to organotin T-125. A 'stabilizer' or 'radical trapping' chemical called butylated hydroxy toluene (BHT) was added to organotin T-125. The MAF laboratory discovered this chemical change, but the laboratory personnel did not know the effect on the final foam. Langley Research Center (LaRC) personnel determined that the BHT could possibly inhibit the catalytic effect of the organotin.

The process for spraying foam on the tank wall structure was also investigated in the chemical processing and materials report. The NCFI 24-124 acreage foam was sprayed using a computer controlled automatic spray system. The BX-250 and BX-265 closeout were sprayed manually with hand-spray devices. The workers were highly skilled and experienced in using these spray devices but they had to spray in high temperature conditions and in enclosed spaces. Automating the spray system to spray in the close-out section might reduce rollover, voids, thin layers, and variability in foam properties.

6.3. Statistical Review of Results

The data provide by MAF has a large amount of scatter. The ET Project reported the average and standard deviation but did not state whether or not the results meet the STP requirements listed in Table 1. A review of the results indicated that the use of an average value along with consideration of the standard deviation left more doubt as to whether or not the requirements were met. To help understand the nature of the data, a statistical review of the results was conducted for the flatwise tension and bondline tension strengths.

6.3.1. Histograms of the Data

Histograms for the flatwise-tension-strength data for the barrel NCFI 24-124 and BX-265 foams are plotted in Figures 15 through 24. The flatwise-tension-strength histograms plots for the ogive NCFI 24-124 foam data were similar to the barrel NCFI 24-124 histogram plots and are not shown. The data is plotted for the various test temperatures (-423°F, -320°F, 75°F, 200°F, and 300°F). The intervals for each histogram in Figures 15 through 19 are based on the minimum and maximum failure loads at each test temperature. In Figures 20 through 24, the intervals are based on the minimum and maximum failure loads over the entire range of test temperatures for each material.

All of the histograms in Figures 15 through 24 exhibit a log normal distribution for both foams. The parameters that define the log normal distribution are listed in Tables 8, 9, and 10 for each test temperature. The probability of the flatwise tension or bondline tension strength for the NCFI 24-124 foam for the ogive and barrel section being greater than 30 psi, using the log normal distribution parameters, is listed in Tables 8 and 9. The probability of the bondline tension strength being greater than 30 psi is low (< 82%) for the ogive NCFI 24-124 foam in Table 8. Also, the flatwise tensile strength has a greater chance (> 90%) of exceeding the 30 psi target strength except at the test temperpature of –423°F (< 63%). The probability of the bondline tension strength being greater than 30 psi is low (< 90%) for the barrel NCFI 24-124 foam in Table 9. Also, the flatwise tensile strength has a greater chance (> 95%) of exceeding the 30 psi strength requirement. The probability of failure, listed in Table 10, for the flatwise tension or bondline tension strength of BX-265 foam being greater than the required tension strength of 35 psi is greater than 99%.

For the higher test temperatures, failure is likely to have occurred in an elastic manner due to softening of the cell wall material. The data that was provided did not contain information on the nature of the failure (i.e. failure surface, slope of the load versus elongation or compression, and displacement) for each test. However, it can be assumed that at cryogenic temperatures the foam failed in a brittle manner due the extreme cold, freezing and stiffening the cell-wall material of the foam. Previous experience and the literature suggests that brittle failure occurs at the lower temperature usually coupled with an increase in failure load [28]. For these materials, there was a slight decrease at the extreme temperature (-423°F). At a test temperature of –423°F, the cell evacuated and there may have been damage in the cellular structure, degrading the strength of the foam. The high-temperature results also follow the trend expected, where the cell wall material softens as the test temperature approaches the glass transition temperature, possibly reducing the strength of the foam.

The plotting of the test result in histograms set a format that provides insight on how the data is related. The test results in the histograms (for both individual and overall test temperatures) also indicate that temperature extremes and test methods play significant role. The peak values for both foams were to the left of the median at cryogenic temperatures. As the temperature increases, the peak shifts to the right of the median. At the elevated temperatures, the peak is to the left of the median. The shift to the left at cryogenic and elevated temperatures suggests that the cell walls are weakened by the temperature effects that reduce the median value.

6.3.2. A-basis and B-basis Material Values

Even with the data tabulated and plotted, there still is uncertainty as to whether or not the requirements established in Table 1 were satisfied. Since this is a human-rated vehicle, evaluation of the data as an A-basis or B-basis material property would suffice. The ET Project provided data with +/- 2 Sigma bounds [29], that is,

$$\pm 2 \text{ Sigma} = \mu \pm 2 \cdot \delta$$

where μ is the mean or average and δ is the standard deviation. This bound is solely based on the mean and standard deviation and does not take into account the number of specimens tested or placed a penalty on the bounds if a low number of samples were tested.

If the use of A-basis or B-basis values for material properties were enforced, the number of samples, regardless of the lot-to-lot values, would play a significant role. The definition of an A-basis material property from Mil-17 Handbook [30] is:

> **A-basis (or A-value)** -- A statistically-based material property; a 95% lower confidence bound on the first percentile of a specified population of measurements. Also a 95% lower tolerance bound for the upper 99% of a specified population.

An alternate definition for an A-basis value is the value exceeded by 99% of the population with 95% confidence for a given sample size. The definition of B-basis material property from Mil-17 Handbook [30] is:

> **B-basis (or B-value)** -- A statistically-based material property; a 95% lower confidence bound on the tenth percentile of a specified population of measurements. Also a 95% lower tolerance bound for the upper 90% of a specified population.

An alternate definition for a B-basis value is the value exceeded by 90% of the population with 95% confidence for a given sample size.

To calculate an A-basis or B-basis material property, the following formula is used:

$$\text{A-basis or B-basis} = \mu - \delta \cdot k_1$$

where k_1 is the tolerance coefficient for a normal distribution given in [31] as

$$k_1 = \frac{z_{1-p} + \sqrt{z_{1-p}^2 - ab}}{a} \tag{6.1}$$

$$a = 1 - \frac{z_{1-\gamma}^2}{2(N-1)}\ ;\ b = z_{1-p}^2 - \frac{z_{1-\gamma}^2}{N} \tag{6.2}$$

N is the sample size and z_{1-p} is the critical value of normal distribution that is exceeded with a probability of 1-p. The values for z_{1-p} and $z_{1-\gamma}$ are defined as

$$\begin{aligned} z_{1-p} &= \alpha\beta\sigma\left[\phi^{-1}\left(1-p\right)\right] \\ z_{1-\gamma} &= \alpha\beta\sigma\left[\phi^{-1}\left(1-\gamma\right)\right] \end{aligned} \tag{6.3}$$

for A-basis: $p = 0.99$

$\gamma = 0.95$

for B-basis: $p = 0.95$

$\gamma = 0.90$

The symbol ϕ^{-1} is the inverse cumulative distribution function for the normal distribution with a specified mean (non-zero) and standard deviation, p is the upper percentage of a specified population, and γ is the percentage of the lower-tolerance band.

The calculated A-basis and B-basis values for the flatwise tension and bondline tension tests for both NCFI 24-124 and BX-265 foams are listed in Tables 8, 9, 10, 11, 12, and 13. In all six of the tables, if the A-basis or B-basis property value is below the required value listed in Table 1 for tension strength, the value is in red and **bold**.

The low number of specimens tested may have effected the A-basis and B-basis values for the NCFI 24-124 foam since there is a penalty if less than 100 specimens are tested. In Tables 8, 9, and 10 the A-basis and B-basis values are listed with the number of specimens tested. The number of specimen tests may not have affected the values of the BX-265 since a large portion of the specimens tested are reported on a lot-to-lot basis. Lots II and III had less than or equal to 90 specimens tested at each test temperature. The total number of BX-265 specimens tested at each temperature was greater than 440 specimens.

The data provided almost always had the average or mean listed with the +/- 2 Sigma value. The –2 Sigma usually provides a "best guess" of what the final B-basis values will be. At first, it was assumed that the –2 Sigma was the low value and the assumed operational value had to be in the range of the standard deviation. This assumption was because of the large degree of scatter and the fact that the –2 Sigma values in some instances were below the required value. In Tables 11, 12, and 13 the A-basis and B-basis values are listed with the average, –2 Sigma, and –3 Sigma values.

Only the B-basis values for room temperature in the results listed in Tables 8 and 11 for the ogive NCFI 24-124 was greater than the required value of 30 psi. The remaining values in the two tables for flatwise and bondline tension strength were all below the required values in Table 1.

The A-basis values for the barrel NCFI 24-124 are always below the –2 Sigma values in Table 9. The B-basis value is below the –2 Sigma for only one instance, when there were only 5 specimens tested (barrel NCFI 24-124, bondline tension at +350°F). For this bondline tension test, both the A-basis and B-basis values are below the –3 Sigma value. This is a further indication that the number of specimen greatly affects the final A-basis or B-basis value.

The calculated A-basis and B-basis values in Tables 9 and 12 indicate that the barrel NCFI 24-124 did not meet the 30 psi requirements as an A-basis material at any temperature for flatwise and bondline tension strength. The flatwise-tension-strength B-basis values for the barrel NCFI 24-124 were also below 30 psi at the elevated temperatures (+200°F and +300°F) and the bondline-tension-strength values were below the required values for all temperatures. There was no indication that the required values in Table 1 were temperature dependent, even though all of the foams are highly temperature dependent.

The A-basis and B-basis values in Tables 10 and 13 for BX-265 satisfied the 35 psi values for all temperatures for both flatwise tension and bondline tension strength. The A-basis values for BX-265 did not satisfy the 35 psi requirement for bondline tension strength

on a lot-to-lot basis. The instances when the values were lower than the required 35 psi were at the temperature extremes (-423°F, -320°F, and +200°F) and where less than 100 specimens were tested.

6.4. Tests for the Reusable Launch Vehicle (RLV) Program

One of the goals for the next generation of launch vehicles is an order of magnitude reduction in the cost of delivering a payload to orbit. Studies on space transportation by NASA indicate that a single-stage-to-orbit (SSTO) reusable launch vehicle (RLV), fueled by LH_2 and LOx has the potential to reach this cost goal. Cryogenic, liquid propellant technology has been investigated such that an RLV would demonstrate efficient, and airline-like operation with seven-day refurbishment cycles between missions to reduce the operational costs and increase safety, thereby reducing the cost to place a payload in orbit. Many of the technologies developed for such high performance cryogenic tanks provide a potential pathway for future enhancements of the Shuttle External Tank. In particular, the recent developments in cryogenic insulation concepts, test and design can be used to help guide the way forward for ET re-design.

Reusable cryogenic tanks for an RLV are required to contain the LH_2 and LOx propellant. Cryogenic insulation development is critical for an RLV because the tanks must function as the primary structure and pressure vessels at both cryogenic temperatures and elevated re-entry temperatures. The cryogenic insulation maintains the quality and quantity of propellant during ground-hold and ascent, and acts as a thermal barrier during re-entry and against thermal soak-through after landing. Candidate cryogenic insulations must be durable, easy to maintain, easy to repair, and reusable for the life of the vehicle.

Cryogenic insulations for an RLV not only must be reusable but may require additional mechanical strength to act as a structural layer. RLV cryogenic insulations are required to minimize boil-off of cryogenic fuels and prevent the liquefaction of air or oxygen on the surface of the vehicle, and eliminate cryopumping to the tank wall, frost or ice build-up, and prevent phase changes of adhesives if TPS is directly bonded to the cryogenic insulation. In the case of RLV, the TPS is an additional layer of insulation over the cryogenic insulation. The lightest through-the-thickness concept for an insulation system is a layered system, where the TPS is directly bonded to the upper surface of the foam. The TPS protects the vehicle during ascent and re-entry where re-entry is the primary load case for sizing the TPS. Other insulation concepts have stand-off TPS over a TPS support structure. The cryogenic insulation and TPS, however, are sized to work in concert for both the ascent and re-entry cases.

Typical cryogenic insulations are closed-cell foams that are sprayed or bonded on to the external surface of the tank. Cryogenic insulations are generally brittle in nature and are prone to cracking under repeated cyclic exposure to thermal stresses induced by temperature gradients and transients, and to membrane and bending stresses due to pressurization loads. The current ET foams do not to endure cyclic repeated thermal and mechanical loading, since the ET is rated to be filled and drained eight times and used only once, while a full-scale RLV tank would potentially be exposed to 1,500 to 2,600 full mission thermal and mechanical cycles. A thorough investigation of the influence of the thermal and mechanical stress conditions on the cryogenic insulation compatibility with the substrate and TPS must be performed. The lifecycle performance of the mechanical and

physical properties and durability also requires thorough test and evaluation. A description of the proposed tests is described in this section.

The Reusable Launch Vehicle (RLV) Program required cryogenic tanks with reusable cryogenic insulation. Additional tests were developed to ensure that the cryogenic insulation will withstand the life cycles the foam insulation is required to endure. A list of these tests is in Table 14. Tests that are currently being used by the ET Project are shaded in grey. Tests that are being used by the ET Project but have additional test parameters for the requirements of the RLV Program are shaded in yellow and **bold**. The cryogenic insulation for the RLV cryogenic tanks was not only to be used as an insulation material but also in some instances as structural foam. The cryogenic insulation will no longer be used as TPS. Additional exterior layers of TPS will be added. The lightest concept is a layered system where the TPS will be directly bonded to upper surface of the foam. Other concepts have stand-off TPS over TPS support structure.

Definitions of the tests used to qualify cryogenic insulation for an RLV are

Thermal conductivity Steady-state liquid nitrogen (LN_2) boil-off (evaporation rate) calorimeter methods were used to determine apparent thermal conductivity (k-value) of insulation material systems at various pressures [32]. The standardized methods for full temperature difference and full-range vacuum conditions established by the Cryogenics Testbed at KSC were employed. Two test apparatus, Cryostat-4 and Cryostat-1, were used at KSC. The Cryostat-4 was used to obtain the comparative k-values. The Cryostat-1 was used to obtain the absolute k-values. Vacuum environments, or cold vacuum pressures (CVP), included the following three basic cases: high vacuum (below $1x10^{-5}$ torr), soft vacuum (1 torr), and no vacuum (760 torr). Additional tests were performed at cold vacuum pressures of $1x10^{-3}$ torr and 100 torr. Nitrogen was the residual gas within the vacuum chamber for all tests. The nominal diameter for all specimens was 20.3 cm (8 in.).

Glass transition temperature A DSC thermal analyzer was used to measure glass transition temperature (T_g) [33]. A heating rate of 20°C/min was used and the T_g was taken at the inflection point of the endotherm. The weight-loss characteristics of the cured foam specimens were measured using a thermogravimetric analyzer (TGA) at a heat-up rate of 2.5°C/min in flowing (40 mL/min) air.

Radiant-heat panel test The flame spread (ASTM E 162, D 3675, and E 648), or ignition/self-extinguishment (FAR 25.853 and ASTM C 542) [33]. The ASTM E 162 and D 3675 method were use to measure downward flame spread on a near vertically mounted specimen (the specimen is tilted 30° from the vertical with the bottom of the specimen further away from the radiant panel than the top of the specimen). ASTM E 648 measures lateral flame spread on a horizontally mounted specimen. The flame spread index, IS, calculated from the ASTM E 162 or D 3675 test data is composed of two factors - a flame spread factor, FS, comparable to an average flame spread rate down the sample surface, and a heat release factor, Q, which represents a measure of the peak heat release rate (HRR). The test is conducted under an incident heat flux that decreases down the length of the sample. FS and Q are coupled parameters – as the burning area increases, the heat released increases. The burning area will increase as the flame spreads along the sample surface. At any moment in time, the larger the burning area, the higher the measure of the heat released will be. Conventional flame

spread tests, such as ASTM E 162 and D 3675, evaluate material performance under specific laboratory conditions and the measured parameters rank material performance relative to other materials.

LO_2 compatibility test The ASTM standard D2512 test simulated the reaction that occurs when two materials collide at various impact energies in a pure oxygen environment at various temperatures and pressures [34]. In the tests at MSFC, a 1.3 cm (0.5 in.) square of a candidate material was placed in an aluminum or stainless-steel cup, which was then filled with liquid or gaseous oxygen. The pressure and temperature were adjusted to simulate the specified conditions. A striker pin was placed in contact with the sample and was then impacted with a 9 Kg (20 lbs.) plummet, which, in combination with the drop-height, produced impact energy of 10 Kg-m (72 ft-lbs.). If the material reacted when impacted, the impact energy was reduced. Twenty samples of the material were impacted and any reaction was noted. A reaction consisted of an audible report, a flash, or evidence of burning. No reaction out of twenty impacts indicated that a material was acceptable for use in the tested oxygen environment. Two or more reactions constituted failure of the sample and indicated that the material was not acceptable for use in the tested oxygen environment. If one reaction out of twenty impacts occurred, the material had to survive forty additional impacts to be acceptable.

Vertical burn test The vertical burn test, FAR 25.853(a) or NASA STD6001, tests a materials resistance to smoke generation and burning [33]. The specimen dimensions were 0.051 m by 0.305 m by 0.025 m and the specimens were placed in a fixture vertically above an igniter. The igniter was lit and burned for 25±5 seconds at a temperature of 1,093°C. The burn length must be less than 0.152 m for the specimen to pass the test.

Cone calorimetry test The cone calorimeter (ASTM E 1354) is a single test method which provides measurements of heat release rate (HRR), specimen mass loss, smoke production, and combustion gases. Measurements include ignitability, HRR, and release rate for smoke, toxic gases, and corrosive products of combustion. Measured properties, such as HRR and smoke generation rate, are obtained for all materials under identical fire exposure conditions. The HRR and other measurements generated from the cone calorimeter can also be used as an input to fire modeling and hazard analysis techniques to evaluate the contribution of the individual components and materials to overall fire safety. Ignition time, time-to-peak HRR, and peak HRR, are measured in the cone calorimeter for various materials.

Oxygen index test The limiting oxygen index test determines a materials resistance to instantaneous combustion in an oxygen rich environment. The test was performed using ASTM standard D-2863 and the specimen had dimensions of 0.051 m by 0.305 m by 0.025 m [33].

Open cell content testing The proportion of closed to open cells in a given insulation quantifies the resistance of the foam to the flow of gases through the foam and the insulation characteristics of the foam [33]. Cryogenic insulations that have high closed cell content inhibited cryopumping or the flow of gases.

Closed cell content measurements are performed according to ASTM D-6226 utilizing a Quantachrome UltraFoam 1000. Closed cell measurements are determined by obtaining the open cell content from Boyle's Law. Boyle's law states that the volume of a gas at constant temperature is inversely proportional to its pressure (V=1/P). Therefore, if a known volume is pressurized in a contained chamber, the decrease in pressure can be correlated to the actual volume and simple mathematics will allow the open cell content to be determined. Once the open cell content is determined, the closed cell content can be obtained.

Moisture absorption Water absorption as specified in MIL-PRF-46194A [35], sections 4.5 (water absorption) and 6.3 (drying) are determined on five specimens selected at random from each density submitted for testing. Each specimen is 2 in. by 2 in. by 1 in. thick (5 cm. by 5 cm. by 2.5 cm.). Each specimen is not sealed or protected with any coating, which would inhibit moisture absorption.

Foam sections and panels are dried in air circulating oven at 250 +/-10°F (121 +/-5°C) for a minimum of 2 hours. Do not allow panels to come in contact with other panels in the oven (do not stack panels). Separate each panel from the closet panel by not less than 1 in. (2.5 cm). Arrange panels parallel to the direction of airflow. Do not place panels directly in the bottom of the oven, or on any other piece of non-perforated metal (which could restrict air flow). Place a piece of perforated metal or heavy metal screen atop the panel to prevent warpage during the drying cycle.

After drying, the specimens are allowed to cool to room temperature (73.4+/-3.6°F) (23.0+/-2.0°C) in an environmentally controlled (50+/- 5% relative humidity) room for 2 hours, and are then weighed. The specimens are placed into an environmentally chamber at a relative humidity of 85+/-2 percent and a temperature of 160+/-5°F (71+/-3°C).

Specimens are removed from the chambers periodically (but at least once a week), allowed to cool to RT, and then reweighed to determine weight after exposure. The above procedure is repeated until the equilibrium moisture level (saturation) is attained. Equilibrium is defined as two consecutive weekly measurements indicating a moisture gain of less than 0.05 percent. Except for reweighing, wet conditioning is not be interrupted. Calculate moisture absorption for each specimen as:

$$\text{Wt. Absorbed\%} = [(\text{Wt. Spec.} - \text{Wt. Dry Spec.})/\text{Wt. Dry Spec.})] \times 100.$$

Cryopumping index test The specimen consists of a 28 cm. by 30.5 cm. substrate with a 28 cm. by 28 cm. by 2.54 cm. square block of cryogenic insulation bonded on the upper surface [32]. Thermocouples are located through-the-thickness of the cryogenic insulation, on the tank wall (inner) surface; in the bondline, and on the upper cryogenic insulation (external) surface. The through-the-thickness thermocouples are located at approximately 0.3175 cm. (1/8 in.) intervals to measure temperature change inside the specimen during the test. The specimen attached over a cryogenic chamber that can hold either LH_2 or LN_2. Cryogen flows into the chamber until steady-state temperatures are achieved (10 to 30 mins.). Once steady-state temperature has been achieved, the cryogen supply is turned off and the inner chamber is heated to room temperature. The cryopumping index is calculated by the following equation

$$CP_{index} = (T_{CP} - T_{SS})/T_{SS}$$

Where CP_{index} is the cryopumping index, T_{CP} is the lowest temperature after the cryogen supply has been turned off, and T_{SS} is the lowest steady-state temperature while the cryogen is flowing into the chamber.

Permeation test No formal tests standard has been developed for this type of testing. Permeation testing on foams was conducted to determine if foams could be used as secondary barrier to prevent H_2 escaping from a leaky graphite-epoxy LH_2 tank. A test similar to the test used at the Rockwell Science Center in Thousand Oaks, CA was utilized [36]. Cups or vessels were placed on either side of the foam. One side was filled with gaseous H_2 at a given pressure while a vacuum was drawn on the other. The gases collected on the vacuum side were placed in a mass spectrometer to determine the species collected in the vacuum. This test also determined the permeation rate for foams.

Compression test Compression specimens were machined to 0.051 m by 0.051 m by 0.025 m dimensions and placed in a servo-hydraulic testing machine. Compression specimens were tested at –253°C, 25°C, and 177°C using ASTM standard D-3574 (E). At 50% of the initial thickness (50% deflection), the load and stress were determined. Load and stress values at 10% deflection were determined from the graph of the deflection versus load for the 50% deflection test

Flatwise tension test Tensile specimens were cut to a dimensions of 0.051 m by 0.051 m by 0.025 m and bonded to support blocks utilizing a low temperature epoxy adhesive. Using ASTM D-1623-C standard, specimens were placed in a servo-hydraulic test stand and loaded in tension to failure.

Shear strength test A 300 mm long by 75 mm wide and 25 mm thick piece of material was bonded to two 50 mm thick steel blocks. The two steel blocks will cause the bonded material to shear when loaded. The ultimate shear strength, was computed simply as the critical load divided by the contact area for this specimen type. The joints between the steel and the core were milled to sharp 90° corners. The specimens were tested in a universal testing machine under controlled displacement rate until fracture using ASTM C273 as the standard. The failure load was taken when one joint started to form a crack between the core and the steel block.

Thermal/Mechanical (1 by 2) or Uniaxial tension tests Combined cyclic thermal and mechanical tests of cryogenic tank wall concepts simulating ring and stringer tanks were performed on two flat 30.5 cm by 61 cm (1 ft. by 2 ft.) panel specimens [37]. A flat specimen closely approximates a tank wall due to the large radius of the tank. These tests were developed from earlier tests of a cryogenic insulation tile developed for the Advanced Launch System (ALS). The purpose of the tests was to simulate both the thermal and mechanical loads experienced in an RLV mission from launch to orbit and to re-entry. This combined cyclic, thermal-mechanical test verified the durability of the cryogenic insulation when subjected to cyclic mission-profile conditions, the bond line integrity between cryogenic insulation and the structure, and the performance of cryogenic tank fabrication technologies on a small-scale.

Thermal/Vibroacoustic Test facilities, Thermal Acoustic Facility and Combined Environments Biaxial Loads Facility, were developed at MSFC to investigate the combined thermal and vibroacoustic effects on TPS tiles and cryogenic insulation.

Large flat specimens (greater than 6 ft. by 6 ft.) simulated a tank or orbiter wall substrate. If the tank wall was being tested, the specimen could be chilled to either –320°F or –423°F or heated to +500°F. The specimen would be loaded in biaxial tension with a mechanical load while being chilled. After certain strain levels and temperatures were achieved, the specimen was placed in front of acoustic horn that could generate a noise level of 172 decibels (dbs).

Thermal Acoustic Facility This facility was developed in 1997 for the X-33 metallic TPS and is capable of duplicating the key acoustic loading and surface temperatures environments representative of the X-33 hypersonic flight. The facility was later modified in 1998 to double the acoustic energy in order test the ET TPS materials. At present this facility can deliver radiant heat from 0 to 30 BTU/ft.^{2}/sec. and up to 172 dbs onto a test article up to six ft. square. The test article currently used for ET TPS testing has a fully characterized dynamic response which closely matches predicted flight responses. Test articles can be thermally conditioned from –423°F using liquid helium to +500°F using gas heaters upon request.

Combined Environments Biaxial Loads Facility The combined environments (CE) facility is able to induce tension or compression loads of up to 1.5 million pounds in each axis onto a flat or curved test article up to 10 ft. square or tanks up to 10 ft. diameter and up to 12 ft. high dome to dome. The ET Project has designed a flat test article for this facility approximately six feet square which results in a uniform 2 to 1 or 1 to 1 strain field which duplicates a pressurized ET side wall or aft dome. The environments from the Thermal Acoustic Facility are then combined with this facility resulting in an ET TPS test facility capable of biaxial loads, acoustics, substrate dynamic response, radiant heat, and substrate cryogenic conditioning.

7. Technology Gaps and Recommendations

The objective of this section is to identify gaps in the technology associated with ET foam characterization and material modeling and to provide general recommendations. The technology gaps are identified by relating typical analysis methods to the current ET test methods and the existing data base of ET foam properties.

The development of a more comprehensive material property database is recommended. The database should include all relevant information about every test specimen with observed anomalies in the data traceable to the original batch from which each specimen was fabricated. The database should be maintained and controlled by appropriate personnel and be easily accessible.

With respect to mechanical properties, it is apparent that the ET foam tests outlined in section 5.1 are not entirely consistent with the range of properties required by the constitutive models and failure criteria of section 4.0. To accurately characterize the foam materials for constitutive model development, additional tests such as outlined in sections 4.0 and 6.4 should be performed over a complete range of environmental conditions. For tension, compression and shear loading, the ET tests should include a method for identifying the transition region, inelastic behavior, and ductile versus brittle failure. Strain-rate sensitivity should be investigated over a range of rates and temperatures consistent with

the application. Failure modes should be clearly identified and with both singular and combined loads investigated to ensure validation of failure criteria. Size and/or scaling effects should be investigated to ensure that the properties measured in laboratory tests are truly representative of the properties found in the acreage foam locations. The applicability of continuum mechanics to the cellular material must be validated through tests that investigate scale and size.

It is recognized that ET foam material processing and application contribute to the total scatter observed in the mechanical property test data. It is also known that both foam density and degree of anisotropy are functions of the spray process and material type. As proposed by Harris[1] there are three ways to account for the resulting material variability. First, these effects may be accounted for by conducting a test matrix that systematically measures the properties of the foam as a function of foam density and location/orientation within the foam. Next, a failure criterion is hypothesized and verified. Then, the failure criterion is used to establish the critical defect requirements. Second, in the absence of a comprehensive materials level test program, a qualification test program that tests representative components in the simulated flight environment should be used to develop an empirical defect acceptance criterion. The qualification test program must be comprehensive to insure that the full range of possible foam properties that can result from the spray process are represented in the data used to establish accept/reject criteria. Third, if the test matrix in either approach, one or two, is not adequate to cover the range of material variability, then knockdown factors should be used to approximate the material variability effects. The magnitude of these knockdown factors may vary according to the degree of conservatism and could be established based on the level of scatter in material property measurements. In the most conservative design approach, the desired factor of safety and the knockdown factor are compounded with the material variability knockdown factor raised to the power of two (or higher) to account for the effect of variation in material fracture toughness properties (K_{IC}) on the critical defect size (a) (section 4.6.2).

It is perhaps most desirable to assume the foam behaves as a continuum and to utilize a fracture mechanics approach to foam failure. The primary concern is establishing the range of applicability of linear elastic fracture mechanics (LEFM). The suitability of the underlying assumptions must be determined by measuring the necessary material properties, applying the fracture models, and validating the models over a range of environmental and loading conditions.

To establish the applicability of LEFM, it is assumed that, over the necessary range of temperatures, the material behaves in a linear elastic manner and that fracture is primarily brittle in nature. The significance of material ductility and any material behavior that could be nonlinear and/or inelastic must be established with respect to the desired fidelity of the fracture model. Additional concerns expressed by Harris[1] include: The fracture toughness tests exhibit little plasticity and satisfy the plastic zone size requirements for LEFM to be valid, fracture toughness material property tests are independent of specimen geometry and exhibit uniform, self-similar crack extension, the failure surfaces of the debris (divots) exhibit similar characteristics to the failure surfaces of the fracture toughness test

[1] C. Harris, "NESC Concerns About ET Foam Debris Acceptance Criteria," NASA Engineering and Safety Center, September 20, 2004.

specimens, and the computed stress intensity factors corresponding to actual divot failures as a function of initial defect (void) size do not vary significantly.

8. Summary

Characterization and modeling of ET foam material has been, and will continue to be, a challenge. In order to provide data for structural analysis methods, it is desirable to consider the foam as a linear elastic continuum material. However, it is apparent that deformation and failure of closed cell foam is primarily governed by behavior at the cellular level and perhaps best described by starting with a micromechanics modeling approach that accounts for anisotropy and variable density. It is also recognized that both deformation and failure are dependent on temperature, strain rate, and loading mode.

This degree of complexity, coupled with the relative lack of quality experimental data, indicates that investigations into the mechanics of ET foam material require a comprehensive, long-term research program. However, the reality of the situation associated with Space Shuttle return to flight dictates that the existing foam material database be coupled with further selected testing and simple analysis methods to provide an acceptable yet safe engineering solution for the near term.

Additional mechanical property testing should be performed to further populate the existing database, paying close attention to the tests required to establish the range of applicability of linear elastic fracture mechanics. The test conditions required to establish constitutive relationships and fracture parameters should be established based on known flight conditions (loads and environments) for all critical locations on the ET. The underlying assumptions necessary to implement these models and parameters into structural analysis should be clearly delineated and related to the accuracy of the structural analysis predictions. This approach should add fidelity to the analysis models, ensure accurate validation of the models, and contribute to the increase in safety of Space Shuttle launch and flight.

9. References

1. MSFC, ET Project - Assured Availability and Maintenance: Critical Requirements Task 4001, FY2001 Report, 2001, September 28, MMC-ET-SE05-650.
2. CAIB, Columbia Accident Investigation Board, Report Volume I, NASA Headquarters, 2003, August.
3. Knight Jr., N. F., Nemeth, M. P., and Hilburger, M. W., Assessment of Technologies for the Space Shuttle External Tank Thermal Protection System and Recommendations for Technology Improvement—Part 2: Structural Analysis Technologies and Modeling Practices, NASA Langley Research Center, 2004, August, NASA/TM-2004-213256.
4. NASA, STS-27R OV-104 Orbiter TPS Damage Review Team: Summary Report, Volume I, 1989, February, NASA-TM-100355-Vol-I.
5. Weiser, E. S., St. Clair, T. L., and Nemeth, M. P., Assessment of Technologies for the Space Shuttle External Tank Thermal Protection System and Recommendations

for Technology Improvement—Part 1: Materials Characterization and Analysis, NASA Langley Research Center, 2004, July, NASA TM-2004-213238.
6. Buras, D., Engineering Process Specifications: Foam Polyurethanes, Spray Application of, Lockheed Martin Space Systems Co., Michoud Operation, 2000, July 20, STP-1513F.
7. Gibson, L. J. and Ashby, M. F., *Cellular Solids - Structure and Properties*, 2nd Edition, Cambridge Solid State Science Series, 1988, Cambridge: Cambridge University Press.
8. Li, X. and Weitsman, Y. J., *Sea Water Effects on Foam-Cored Composite Sandwich Layups,* 2004.
9. Brezny, R. and Green, D. J., *The Effect of Cell Size on the Mechanical Behavior of Cellular Materials.* Acta Metall. Mater., 1990, **38**(12): p. 2517-2526.
10. Bazant, Z. P., et al., *Size Effect and Asymptotic Matching Analysis of Fracture of Closed-Cell Polymeric Foam,* International Journal of Solids and Structures, 2003, **40**: p. 7197-7217.
11. Viana, G. M. and Carlsson, L. A., *Influences of Foam Density and Core Thickness on Debond Toughness of Sandwich Specimens with PVC Foam Core,* Journal of Sandwich Structures and Materials, 2003, **5**: p. 103-118.
12. Viana, G. M. and Carlsson, L. A., *Mechanical Properties and Fracture Characterization of Cross-linked PVC Foams,* Journal of Sandwich Structures and Materials, 2002, **4**: p. 99-113.
13. Gdoutos, E. E., Daniel, I. M., and Wang, K. A., *Failure of Cellular Foams Under Multiaxial Loading,* Composites, Part A: Applied Science and Manufacturing, 2002, **33**: p. 163-176.
14. Gdoutos, E. E., Daniel, I. M., and Wang, K. A., *Multiaxial Characterization and Modeling of a PVC Cellular Foam,* Journal of Thermoplastic Composite Materials, 2001, **14**: p. 365-373.
15. Tsai, S. W. and Wu, E. M., *A General Theory of Strength for Anisotropic Materials,* Journal of Composite Materials, 1971, **5**: p. 58-80.
16. Christensen, R. A., Freeman, D. C., and DeTeresa, S. J., *Failure Criteria for Isotropic Materials, Applications to Low-Density Types,* International Journal of Solids and Structures, 2002, **39**: p. 973-982.
17. Benderly, D. and Putter, S., *Characterization of the Shear/Compression Failure Envelope of Rohacell Foam.* Polymer Testing, 2003, **23**: p. 51-57.
18. Theocaris, P. S., *Failure Modes of Closed-Cell Polyurethane Foams,* International Journal of Fracture, 1992, **56**: p. 353-375.
19. Abernethy, R. B., *The New Weibull Handbook,* 1994.
20. Todinov, M. T., *Statistics of Defects in One-Dimensional Components,* Computational Materials Science, 2002, **24**: p. 430-442.
21. Paul, A., Seshacharyulu, T., and Ramamurty, U., *Tensile Strength of a Closed-Cell Al Foam in the Presence of Notches and Holes,* Scripta Materialia, 1999, **40**(7): p. 809-814.
22. Grenestedt, J. L., Hallstrom, S., and Kuttenkeuler, J., *On Cracks Emanating From Wedges in Expanded PVC Foam,* Engineering Fracture Mechanics, 1996, **54**(4): p. 445-456.
23. Andrews, E. W. and Gibson, L. J., *On Notch-Strengthening and Crick Tip Deformation in Cellular Metals,* Materials Letters, 2002, **57**: p. 532-536.

24. Olurin, O. B., Fleck, N. A., and Ashby, M. F., *Deformation and Fracture of Aluminum Foams,* Materials Science and Engineering A, 2000, **A291**: p. 136-146.
25. Smith, R. A., Materials in Engineering Applications, 1978, **1**: p. 121-128.
26. Choi, S. and Sankar, B. V., *Fracture Toughness of Carbon Foam,* Journal of Composite Materials, 2003, **37**(23): p. 2101-2116.
27. Jerman, G., *BX265 Polyurethane Foam Fracture Analysis*, 2004, NASA, MSFC.
28. Johnson, T. F. and Gates, T. S., *High Temperature Polyimide Materials in Extreme Temperature Environments,* in *AIAA 42nd Annual AIAA/ASME/ASCE/AHS/ASC Structures, Structural Dynamics, and Materials Conference*, AIAA-2001-1214, 2001, Seattle, WA.
29. Ang, A. H.-S. and Tang, W. H., *Probability Concepts in Engineering Planning and Design, Volume I-Basic Principles*, 1975, New York: John Wiley & Sons, Inc.
30. MIL-HDBK-17-1F, *Composite Materials Handbook, Volume 1, Polymer Matrix Composites Guidelines for Characterization of Structural Materials*, Dept. of Defense, Editor, 2002, Volume 1.
31. NIST/SEMATECH, *e-Handbook of Statistical Methods*.
32. Johnson, T. F., Weiser, E. S., Grimsley, B. W., and Jensen, B. J., *Cryopumping in Cryogenic Insulations for a Reusable Launch Vehicle*. in *48th International SAMPE Symposium and Exhibition,* 2003, Long Beach, CA.
33. Weiser, E. S., Johnson, T. F., St. Clair, T. L., Echigo, Y., Kaneshiro, H., and Grimsley, B.W., *Polyimide Foams for Aerospace Vehicles,* Journal of High Performance Polyimides, 2000, **Volume 12**: p. 1-12.
34. NASA, *Flammability, Odor, Offgassing, and Compatibility Requirements and Test Procedures for Material in Environments that Support Combustion*, NASA, Editor, 1991, Handbook 8060.1C (NHB 8060.1C).
35. DOE, *Performance Specification, Foam, Rigid, Structural, Closed Cell*, 1997, MIL-PRF-46194A, Military Specifications and Standards.
36. Robinson, M. J., *Composite Cryogenic Propellant Tank Development*, in *35th AIAA/ASME/ASCE/AHS/ASC Structures, Structural Dynamics and Materials Conference,* 1994, Hilton Head, SC.
37. Johnson, T. F., Natividad, R., Rivers, H. K., and Smith, R., Thermal Structures Technology Development for Reusable Launch Vehicle Cryogenic Propellant Tanks, 2005, August, NASA/TM-2005-213913.

10. Tables

Table 1. STP requirements and processing parameters for the ET TPS materials.

Test Parameters	NCFI 124-24 (STP 1535 & STM L1A5)	NCFI 124-57 (STP 1535 & STM L1A2)	BX-250 (STP 1513F & STM L742-2)	SS-1171 (STP 1536 & STM L1A6-1)	BX-265 (STP 1540 & STM L1B3)	PDL-1034 (STP 1532 & STM L1A1)
Pumping ratio (avg. by vol.)	1.91 – 2.09 to 1	1.91 – 2.09 to 1	0.98 – 1.08 to 1	0.95 – 1.05 to 1	0.95 – 1.05 to 1	(1.08 to 1.12 to 1 by wt.
Density	2.0 – 2.5 lbs/ft.	2.6 – 3.1 lbs/ft.	1.8 – 2.6 lbs/ft. (1.8 – 3.0 lbs/ft. with multiple knitlines)	1.8 – 2.6 lbs/ft. (1.8 – 3.0 lbs/ft. with multiple knitlines)	1.8 – 2.6 lbs/ft. (1.8 – 3.0 lbs/ft. with multiple knitlines)	2.3 – 3.1 lbs/ft.
Density, Intertank	2.0 – 2.8 lbs/ft.					
Tensile strength	30 psi min.	40 psi min.	35 psi min.	35 psi min.	35 psi min.	35 psi min.
Component temp. (avg.)	135±5°F	135±5°F	110±10°F	135 – 150°F	145 – 160°F	70 – 80°F
Component temp. (avg.)	125 – 145°F	125 – 145°F				
Substrate temp.	125 – 160°F	105 – 130°F	65 – 100°F	70 – 100°F	70 – 100°F	65 – 110°F
Substrate temp. Ablator	90 – 160°F	90 – 130°F				
Room temp.	85 – 105°F	85 – 105°F	65 – 100°F	70 – 100°F	70 – 100°F	65 – 110°F
Relative humidity	5 - 30%	5 - 30%	10 - 60%	10 - 60%	10 - 60%	10 - 70%
Overlap-time	7 – 28 sec.	7 – 21 sec.	45 sec. max.	45 sec. max.	45 sec. max.	
Overlap-time, Intertank	7 – 21 sec.					

Note: Monostrain test determines the derived properties such as ultimate strain, failure stress, Young's modulus, and coefficient of thermal expansion (CTE) in $\alpha\Delta T$.

Table 2. Material characterization and qualification tests.

Test no.	Test name	Standard	Test temperature (°F)						
			-423	-320	RT (+75)	+100	+200	+300	+350
1	Density	ASTM D1622			x				
2	Plug pull	TTP-13M50FT			x				
3	Lap shear	TTP-2007			x			x	
4	Flexure	TTP-2006			x				
5	Compression	ASTM D1621			x				
6	Bond tension	ASTM D1623	x	x	x	x	x	x	x
7	Monostrain	TTP-2002	x	x	x	x	x	x	x
8	Cryoflex	EQTP 1002 Gradient	x						
9	Poisson's ratio	TTP-2003			x				
10	Thermal conductivity	ASTM C177	x	x	x				
11	Specific heat	ASTM E1269	x	x	x				

Table 3. NCFI 24-124 acreage foam material property data for the ogive section of an ET LOx tank.

Test temp. (°F)	Data value	Monostrain data				Bond tension (psi	Flatwise tension (psi)	Comp. (psi)	Density (pcf)
		αΔT (in./in.)	Ult. strain (in./in.)	Failure stress (psi)	Young's modulus (psi)				
-423	High					56.3	66.0		
	Avg.					35.8	33.6		
	Low					24.8	11.3		
	Stand. dev.					7.8	8.7		
	+2 Sigma					**51.4**	**51.1**		
	-2 Sigma					20.2	**16.1**		
	No. of Spec.					40	121		
-320	High					57.8	73.5		
	Avg.					39.0	44.1		
	Low					15.0	13.8		
	Stand. dev.					10.0	10.4		
	+2 Sigma					59.0	**64.8**		
	-2 Sigma					**19.0**	**23.4**		
	No. of Spec.					44	118		
+72	High					70.8	66.5	41.80	2.36
	Avg.					41.7	48.7	33.89	2.19
	Low					11.3	18.0	29.50	1.98
	Stand. dev.					15.8	9.5	2.39	0.08
	+2 Sigma					73.3	67.8	**38.7**	**2.4**
	-2 Sigma					10.1	**29.7**	29.1	**2.0**
	No. of Spec.					41	121	125	125
+200	High					55.8	62.8		
	Avg.					38.2	38.8		
	Low					14.5	23.8		
	Stand. dev.					10.9	6.9		
	+2 Sigma					59.9	**52.7**		
	-2 Sigma					**16.5**	**24.9**		
	No. of Spec.					45	117		
+300	High					48.3	45.0		
	Avg.					28.4	26.4		
	Low					18.8	12.5		
	Stand. dev.					6.4	6.8		
	+2 Sigma					**41.2**	**39.9**		
	-2 Sigma					15.6	**12.8**		
	No. of Spec.					44	121		
+350	High					56.3	66.0		
	Avg.					35.8	33.6		
	Low					24.8	11.3		
	Stand. dev.					7.8	8.7		
	+2 Sigma					**51.4**	**51.1**		
	-2 Sigma					20.2	**16.1**		
	No. of Spec.					40	121		

Note: The red or **bold** +/- 2 Sigma data indicates that the high or low values are higher or lower than the +/- 2 Sigma values respectively.

Table 4. NCFI 24-124 acreage foam material property data for the barrel section of an ET LO_2 tank.

Test temp. (°F)	Data value	Monostrain data				Bond tension (psi	Flatwise tension (psi)	Comp. (psi)	Density (pcf)
		αΔT (in./in.)	Ult. strain (in./in.)	Failure stress (psi)	Young's modulus (psi)				
-423	High					50.5	55.8		
	Avg.					33.6	41.8		
	Low					23.3	28.0		
	Stand. dev.					5.8	6.7		
	+2 Sigma					**45.2**	**55.3**		
	-2 Sigma					21.9	**28.3**		
	No. of Spec.					94	39		
-320	High					65.8	72.3		
	Avg.					43.3	49.6		
	Low					20.0	26.8		
	Stand. dev.					9.7	10.4		
	+2 Sigma					**62.6**	**70.4**		
	-2 Sigma					**24.0**	**28.7**		
	No. of Spec.					99	36		
+72	High					48.3	58.8	35.30	2.39
	Avg.					28.4	44.1	30.57	2.26
	Low					18.8	29.0	26.00	2.18
	Stand. dev.					6.4	7.3	2.34	0.05
	+2 Sigma					**41.2**	**58.6**	**35.3**	2.4
	-2 Sigma					15.6	**29.5**	25.9	2.2
	No. of Spec.					44	38	100	100
+200	High					58.5	53.8		
	Avg.					40.5	40.4		
	Low					20.0	23.8		
	Stand. dev.					7.6	7.0		
	+2 Sigma					**55.7**	54.3		
	-2 Sigma					**25.4**	**26.5**		
	No. of Spec.					96	39		
+300	High					46.3	48.2		
	Avg.					32.9	33.4		
	Low					20.5	24.3		
	Stand. dev.					5.8	5.2		
	+2 Sigma					**44.5**	**43.8**		
	-2 Sigma					**21.4**	23.0		
	No. of Spec.					97	39		
+350	High					28.3			
	Avg.					24.7			
	Low					19.8			
	Stand. dev.					3.7			
	+2 Sigma					32.1			
	-2 Sigma					17.2			
	No. of Spec.					5			

Note: The red or **bold** +/- 2 sigma data indicates that the high or low values are higher or lower than the +/- 2 sigma values respectively.

Table 5. Reported NCFI 24-124 acreage foam material property data for the barrel section of an ET LO_2 tank separated by lots.

Test temp. (°F)	Data value	Bond tension (psi)			Flatwise tension (psi)			Compression (psi)			Density (pcf)		
		Total	Lot 2	Lot 3	Total	Lot 2	Lot 3	Total	Lot 2	Lot 3	Total	Lot 2	Lot 3
-423	High	50.5	43.5	50.5	55.8	55.8	53.8						
	Avg.	33.6	33.5	33.6	41.8	41.9	41.7						
	Low	23.3	23.3	25.0	28.0	29.5	28.0						
	Stand. dev.	5.8	6.1	5.6	6.7	7.0	6.7						
	+2 Sigma	**45.2**	45.8	**44.8**	**55.3**	55.9	55.0						
	-2 Sigma	21.9	21.3	22.4	**28.3**	28.0	**28.3**						
	No. of Spec.	94	45	49	39	19	20						
-320	High	65.8	61.5	65.8	72.3	59.3	72.3						
	Avg.	43.3	39.3	47.4	49.6	45.4	52.6						
	Low	20.0	20.0	25.0	26.8	26.8	31.5						
	Stand. dev.	9.7	9.7	7.7	10.4	7.3	11.2						
	+2 Sigma	**62.6**	**58.7**	**62.8**	**70.4**	60.0	75.1						
	-2 Sigma	**24.0**	19.8	**32.0**	**28.7**	**30.7**	30.2						
	No. of Spec.	99	50	49	36	18	18						
+72	High	48.3	39.0	48.3	58.8	54.0	58.8	35.30	35.30	31.00	2.39	2.39	2.33
	Avg.	28.4	28.3	28.5	44.1	41.0	47.4	30.57	32.55	28.58	2.26	2.28	2.25
	Low	18.8	20.8	18.8	29.0	29.0	38.5	26.00	29.80	26.00	2.18	2.19	2.18
	Stand. dev.	6.4	6.0	6.7	7.3	7.6	5.2	2.34	1.25	1.21	0.05	0.04	0.04
	+2 Sigma	**41.2**	40.4	**41.9**	**58.6**	56.3	**57.8**	**35.3**	**35.1**	**31.0**	2.4	**2.4**	2.3
	-2 Sigma	15.6	16.2	15.1	**29.5**	25.8	37.0	25.9	**30.1**	**26.2**	2.2	2.2	2.2
	No. of Spec.	44	15	29	38	20	18	100	50	50	100	50	50
+200	High	58.5	58.5	50.5	53.8	50.0	53.8						
	Avg.	40.5	43.8	37.1	40.4	36.4	44.2						
	Low	20.0	29.8	20.0	23.8	23.8	34.6						
	Stand. dev.	7.6	6.9	6.8	7.0	7.0	4.4						
	+2 Sigma	**55.7**	**57.7**	50.7	54.3	50.3	**53.1**						
	-2 Sigma	**25.4**	**29.9**	**23.6**	**26.5**	22.4	**35.3**						
	No. of Spec.	96	49	47	39	19	20						
+300	High	46.3	46.3	43.5	48.2	39.5	48.2						
	Avg.	32.9	32.7	33.1	33.4	30.7	35.9						
	Low	20.5	20.5	25.0	24.3	24.3	29.5						
	Stand. dev.	5.8	6.8	4.7	5.2	4.2	4.8						
	+2 Sigma	**44.5**	**46.2**	**42.5**	**43.8**	**39.0**	**45.6**						
	-2 Sigma	**21.4**	19.1	23.8	23.0	22.3	26.3						
	No. of Spec.	97	48	49	39	19	20						
+350	High	28.3	0.0	28.3									
	Avg.	24.7	0.0	24.7									
	Low	19.8	0.0	19.8									
	Stand. dev.	3.7	0.0	3.7									
	+2 Sigma	32.1	0.0	32.1									
	-2 Sigma	17.2	0.0	17.2									
	No. of Spec.	5	0	5									

Note: The red or **bold** +/- 2 Sigma data indicates that the high or low values are higher or lower than the +/- 2 Sigma values respectively.

Table 6. BX-250 closeout foam material property data for the ET.

Test temp. (°F)	Data value	Monostrain data				Bond tension (psi	Flatwise tension (psi)	Comp. (psi)	Density (pcf)
		αΔT (in./in.)	Ult. strain (in./in.)	Failure stress (psi)	Young's modulus (psi)				
-423	High	-0.02290	0.02680	85.5	3596.0	63.9		89.6	
	Avg.	-0.01870	0.02180	53.6	2566.5	52.6		75.6	
	Low	-0.01230	0.01650	39.0	1766.7	41.3		61.6	
	Stand. dev.								
-320	High	-0.01970	0.03180	63.7	2546.9	72.7		92.3	
	Avg.	-0.01780	0.02710	54.9	2160.9	65.4		77.4	
	Low	-0.01380	0.02180	32.4	1837.2	58.1		62.5	
	Stand. dev.								
+72	High	-0.01160	0.05800	60.4	1616.9	81.3		55.20	
	Avg.	-0.01010	0.04170	51.1	1368.7	69.3		50.20	
	Low	-0.00680	0.03400	37.4	1161.4	57.3		45.20	
	Stand. dev.								
+100	High	0.00000	0.19360	47.7	1253.2	82.3		46.40	2.72
	Avg.	0.00000	0.14540	42.3	1061.5	75.4		41.90	2.15
	Low	0.00000	0.09990	34.8	847.8	68.5		37.40	1.73
	Stand. dev.								
+200	High	N/A	0.27390	30.2	711.0	56.1		32.4	
	Avg.	N/A	0.22700	25.2	391.2	47.4		30.1	
	Low	N/A	0.20500	21.9	154.4	38.7		27.8	
	Stand. dev.								

Table 7. BX-265 closeout foam material property data for the ET.

Test temp. (°F)	Data value	Monostrain data				Bond tension (psi	Flatwise tension (psi)	Comp. (psi)	Density (pcf)
		αΔT (in./in.)	Ult. strain (in./in.)	Failure stress (psi)	Young's modulus (psi)				
-423	High	0.02366	0.03412	89.5	3495.1	137.5	131.5		
	Avg.	0.02018	0.02450	48.3	1589.8	73.9	70.7		
	Low	0.01228	0.01442	20.1	629.5	27.3	41.8		
	Stand. dev.	0.00159	0.00332	9.8	449.4	16.8	12.8		
	+2 Sigma	**0.02337**	**0.03113**	**67.9**	**2488.7**	**107.5**	**96.3**		
	-2 Sigma	**0.01700**	**0.01787**	**28.8**	**690.9**	**40.3**	**45.0**		
	No. of Spec.	184	184	184	184	466	170		
-320	High	0.02109	0.03993	84.2	3042.3	141.3	140.5		
	Avg.	0.01812	0.02804	52.7	1407.4	87.8	84.1		
	Low	0.01219	0.01887	35.5	630.7	31.5	53.0		
	Stand. dev.	0.00161	0.00409	9.7	352.8	19.2	17.1		
	+2 Sigma	0.02134	**0.03622**	**72.1**	**2113.0**	**126.3**	**118.3**		
	-2 Sigma	**0.01489**	**0.01987**	33.2	**701.9**	**49.3**	49.9		
	No. of Spec.	131	131	131	131	470	167		
+72	High	0.00000	0.23460	53.1	1404.2	101.0	105.0	54.53	3.19
	Avg.	0.00000	0.13209	42.5	964.8	79.5	88.5	42.85	2.38
	Low	0.00000	0.05653	32.4	648.0	30.8	59.0	27.94	2.00
	Stand. dev.	0.00000	0.02833	3.6	118.2	12.6	6.7	4.75	0.19
	+2 Sigma	0.00000	**0.18875**	**49.8**	**1201.1**	104.6	**101.9**	**52.34**	**2.76**
	-2 Sigma	0.00000	**0.07543**	**35.3**	**728.4**	**54.3**	**75.0**	**33.35**	2.00
	No. of Spec.	212	212	212	212	540	166	469	469
+200	High	0.04209	0.32447	37.4	650.0	73.8	74.8		
	Avg.	0.02132	0.22545	28.9	271.3	53.1	58.2		
	Low	0.00524	0.06577	15.9	128.1	23.5	39.8		
	Stand. dev.	0.00812	0.03712	3.3	107.8	8.3	6.5		
	+2 Sigma	**0.03756**	**0.29968**	**35.4**	**486.9**	**69.7**	**71.2**		
	-2 Sigma	0.00508	**0.15121**	**22.4**	55.7	**36.5**	**45.2**		
	No. of Spec.	138	138	138	138	448	158		

Note: The red or **bold** +/- 2 Sigma data indicates that the high or low values are higher or lower than the +/- 2 Sigma values respectively.

Table 8. Ogive NCFI 24-124 acreage foam material log normal distribution values and A-basis and B-basis property values.

Test	Test temp. (°F)	Average stress (psi)	Standard deviation (psi)	Number of specimen	COV	λ	Probability > 30 psi (%)	A-basis (psi)	B-basis (psi)
Flatwise tension	-423	33.60	8.74	121	0.260098	3.48075	62.01	**10.5**	**20.5**
	-320	44.08	10.35	118	0.234863	3.758418	93.59	**16.7**	**28.5**
	75	48.73	9.52	121	0.195459	3.867137	99.14	**23.5**	34.4
	200	38.84	6.95	117	0.17894	3.643335	91.20	**20.4**	**28.4**
	300	26.35	6.79	121	0.257614	3.238333	26.36	**8.4**	**16.2**
Bondline tension	-423	35.77	7.79	40	0.217886	3.553442	75.76	**12.9**	**22.6**
	-320	38.98	10.01	44	0.256654	3.630218	81.39	**10.0**	**22.3**
	75	41.70	15.80	41	0.378809	3.658812	75.18	**-4.5**	**15.1**
	200	38.16	10.85	45	0.284371	3.601296	75.92	**6.8**	**20.1**
	300	28.43	6.40	44	0.225052	3.322105	36.26	**9.9**	**17.8**

Note: The red or **bold** A-basis or B-basis property values indicate that the values were less than the required values listed in Table 1.

Table 9. Barrel NCFI 24-124 acreage foam material log normal distribution values and A-basis and B-basis property values.

Test	Test temp. (°F)	Average stress (psi)	Standard deviation (psi)	Number of specimen	COV	λ	Probability > 30 psi (%)	A-basis (psi)	B-basis (psi)
Flatwise tension	-423	41.79	6.73	39	0.161096	3.719798	97.60	**22.0**	30.4
	-320	49.58	10.42	36	0.210107	3.881526	98.89	**18.6**	31.7
	75	44.06	7.25	38	0.164659	3.771948	98.78	**22.7**	31.7
	200	40.39	6.96	39	0.172442	3.683708	94.93	**19.9**	**28.6**
	300	33.37	5.20	39	0.155928	3.495554	72.75	**18.1**	**24.5**
Bondline tension	-423	33.56	5.83	94	0.173817	3.498248	71.17	**17.9**	**24.6**
	-320	43.31	9.66	99	0.222946	3.743603	93.77	**17.4**	**28.6**
	75	28.43	6.40	44	0.225052	3.322105	36.26	**9.9**	**17.8**
	200	40.54	7.59	96	0.187132	3.684718	93.51	**20.1**	**28.9**
	300	32.91	5.78	97	0.175587	3.478465	67.00	**17.4**	**24.1**
	350	24.68	3.73	5	0.150939	3.194602	8.55	**3.3**	**12.1**

Note: The red or **bold** A-basis or B-basis property values indicate that the values were less than the required values listed in Table 1.

Table 10. BX-265 closeout foam material log normal distribution values and A-basis and B-basis property values.

Test	Test temp. (°F)	Average stress (psi)	Standard deviation (psi)	Number of specimen	COV	λ	Probability > 35 psi (%)	A-basis (psi)	B-basis (psi)
Flatwise tension (Total)	-423	70.68	12.82	170	0.181336	4.241755	99.99	37.5	51.9
	-320	84.11	17.10	167	0.203271	4.411457	100.00	39.8	59.1
	75	88.48	6.72	166	0.075942	4.479949	100.00	71.1	78.6
	200	58.21	6.49	158	0.111499	4.057876	100.00	41.3	48.7
Bondline tension (Lot I)	-423	73.91	17.81	168	0.227326	4.277059	99.93	**32.2**	50.6
	-320	87.85	20.58	170	0.21911	4.451578	100.00	40.1	61.1
	75	79.47	11.25	223	0.158378	4.3629	100.00	48.4	62.1
	200	53.06	7.11	177	0.1564	3.959272	99.51	**32.5**	41.5
Bondline tension (Lot II)	-423	72.61	21.84	88	0.245275	4.255086	99.78	**26.5**	46.5
	-320	91.61	21.76	90	0.224601	4.492321	100.00	38.3	61.5
	75	75.18	11.47	88	0.149571	4.308751	100.00	46.5	59.0
	200	50.18	9.44	77	0.141735	3.905616	99.33	**31.8**	39.8
Bondline tension (Lot III)	-423	83.23	12.92	90	0.262363	4.387226	99.92	**24.1**	49.6
	-320	87.04	12.67	90	0.250053	4.43506	99.98	**28.2**	53.6
	75	88.38	11.53	88	0.129815	4.473163	100.00	57.3	70.7
	200	53.88	7.87	86	0.175189	3.971411	99.12	**28.0**	39.1
Bondline tension (Lot IV)	-423	70.22	10.13	120	0.183983	4.234661	99.99	35.3	50.3
	-320	81.12	18.15	120	0.156186	4.38376	100.00	46.9	61.6
	75	78.84	12.77	140	0.146187	4.356783	100.00	47.6	61.1
	200	52.38	7.44	108	0.150217	3.947258	99.55	**31.0**	40.2
Bondline tension (Total)	-423	71.67	16.80	466	0.141301	4.262101	100.00	44.9	56.5
	-320	88.16	19.25	470	0.205908	4.457983	100.00	40.1	60.9
	75	81.11	12.59	539	0.157441	4.383443	100.00	47.7	62.2
	200	57.75	8.30	448	0.128774	4.047832	99.99	37.9	46.5

Note: The red or **bold** A-basis or B-basis property values indicate that the values were less than the required values listed in Table 1.

Table 11. Comparison of A-basis and B-basis values to –2 Sigma and –3 Sigma values for NCFI 24-124 acreage foam on the ogive section.

Test	Test temp. (°F)	Average stress (psi)	A-basis (psi)	B-basis (psi)	-2 Sigma (psi)	-3 Sigma (psi)	A-basis Less than	B-basis Less than
Flatwise tension	-423	33.60	**10.5**	**20.5**	16.12	7.38	-2 Sigma	-
	-320	44.08	**16.7**	**28.5**	23.37	13.02	-2 Sigma	-
	75	48.73	**23.5**	34.4	29.68	20.15	-2 Sigma	-
	200	38.84	**20.4**	**28.4**	24.94	17.99	-2 Sigma	-
	300	26.35	**8.4**	**16.2**	12.77	5.99	-2 Sigma	-
Bondline tension	-423	35.77	**12.9**	**22.6**	20.18	12.39	-2 Sigma	-
	-320	38.98	**10.0**	**22.3**	18.97	8.97	-2 Sigma	-
	75	41.70	**-4.5**	**15.1**	10.11	-5.69	-2 Sigma	-
	200	38.16	**6.8**	**20.1**	16.46	5.60	-2 Sigma	-
	300	28.43	**9.9**	**17.8**	15.63	9.24	-2 Sigma	-

Note: The red or **bold** A-basis or B-basis property values indicate that the values were less than the required values listed in Table 1.

Table 12. Comparison of A-basis and B-basis values to –2 Sigma and –3 Sigma values for NCFI 24-124 acreage foam on the barrel section.

Test	Test temp. (°F)	Average stress (psi)	A-basis (psi)	B-basis (psi)	-2 Sigma (psi)	-3 Sigma (psi)	A-basis Less than	B-basis Less than
Flatwise tension	-423	41.79	**22.0**	30.4	28.33	21.60	-2 Sigma	-
	-320	49.58	**18.6**	31.7	28.75	18.33	-2 Sigma	-
	75	44.06	**22.7**	31.7	29.55	22.29	-2 Sigma	-
	200	40.39	**19.9**	**28.6**	26.46	19.50	-2 Sigma	-
	300	33.37	**18.1**	**24.5**	22.96	17.76	-2 Sigma	-
Bondline tension	-423	33.56	**17.9**	**24.6**	21.89	16.06	-2 Sigma	-
	-320	43.31	**17.4**	**28.6**	24.00	14.34	-2 Sigma	-
	75	28.43	**9.9**	**17.8**	15.63	9.24	-2 Sigma	-
	200	40.54	**20.1**	**28.9**	25.37	17.78	-2 Sigma	-
	300	32.91	**17.4**	**24.1**	21.36	15.58	-2 Sigma	-
	350	24.68	**3.3**	**12.1**	17.23	13.50	Both	Both

Note: The red or **bold** A-basis or B-basis property values indicate that the values were less than the required values listed in Table 1.

Table 13. Comparison of A-basis and B-basis values to –2 Sigma and –3 Sigma values for BX-265 closeout foam.

Test	Test temp. (°F)	Average stress (psi)	A-basis (psi)	B-basis (psi)	-2 Sigma (psi)	-3 Sigma (psi)	A-basis Less than	B-basis Less than
Flatwise tension	-423	70.68	37.5	51.9	45.05	32.23	-2 Sigma	-
	-320	84.11	39.8	59.1	49.92	32.82	-2 Sigma	-
	75	88.48	71.1	78.6	75.05	68.33	-2 Sigma	-
	200	58.21	41.3	48.7	45.23	38.74	-2 Sigma	-
Bondline tension (Lot I)	-423	73.91	**32.2**	50.6	36.99	19.18	-2 Sigma	-
	-320	87.85	40.1	61.1	50.46	29.88	-2 Sigma	-
	75	79.47	48.4	62.1	52.69	41.45	-2 Sigma	-
	200	53.06	**32.5**	41.5	35.96	28.84	-2 Sigma	-
Bondline tension (Lot II)	-423	72.61	**26.5**	46.5	39.56	17.72	-2 Sigma	-
	-320	91.61	38.3	61.5	43.51	21.75	-2 Sigma	-
	75	75.18	46.5	59.0	65.43	53.96	Both	-2 Sigma
	200	50.18	**31.8**	39.8	35.00	25.56	-2 Sigma	-
Bondline tension (Lot III)	-423	83.23	**24.1**	49.6	44.38	31.46	-2 Sigma	-
	-320	87.04	**28.2**	53.6	55.78	43.11	Both	-2 Sigma
	75	88.38	57.3	70.7	55.79	44.27	-2 Sigma	-
	200	53.88	**28.0**	39.1	36.64	28.78	Both	-
Bondline tension (Lot IV)	-423	70.22	35.3	50.3	51.42	41.29	-2 Sigma	-2 Sigma
	-320	81.12	46.9	61.6	51.86	33.70	-2 Sigma	-
	75	78.84	47.6	61.1	55.57	42.80	-2 Sigma	-
	200	52.38	**31.0**	40.2	42.88	35.44	Both	-2 Sigma
Bondline tension (Total)	-423	71.67	44.9	56.5	40.31	23.51	-2 Sigma	-
	-320	88.16	40.1	60.9	49.35	30.10	-2 Sigma	-
	75	81.11	47.7	62.2	54.30	41.71	-2 Sigma	-
	200	57.75	37.9	46.5	36.47	28.17	-	-

Note: The red or **bold** A-basis or B-basis property values indicate that the values were less than the required values listed in Table 1.

Table 14. Material characterization and qualification tests for an RLV.

Test type	Test no.	Test name	Standard	Test temperature (°F)					
				-423	-320	RT (+75)	+250	+350	+450
Thermal physical	1	**Thermal conductivity**	ASTM C177, ASTM C518	x	x	x	x	x	x
	2	Specific heat	ASTM E1269	x	x	x	x	x	x
	3	Glass transition (T_g)	DSC						
Flame resistance	4	Radiant heat panel	ASTM E162				x	x	x
	5	LOx compatibility	ASTM D2512		x	x			x
	6	Vertical burn	NASA STD6001, FAR 25-853 (a)			x			
	7	Cone calorimetry	ASTM E1354			x			
	8	Oxygen index	ASTM D2863			x			
Physical	9	Open cell content	ASTM D6226			x			
	10	Moisture absorption	MIL-PRF-46194A, Sects. 4.5, 6.3			x	x	x	x
	11	Cryopumping index	No standard	x	x				
	12	Permeation		x	x	x			
	13	Density	ASTM D1622			x			
Mechanical	14	Plug pull	TTP-13M50FT			x			
	15	Lap shear	TTP-2007			x			
	16	Flexure	TTP-2006	x	x	x			
	17	**Compression**	ASTM D1621, ASTM D3574 (E)	x	x	x	x	x	x
	18	Bond tension	ASTM D1623	x	x	x	x	x	x
	19	**Flatwise tension**	ASTM C297, ASTM D1623 (C)	x	x	x	x	x	x
	20	Poisson's ratio	TTP-2003			x			
	21	Monotrain*	TTP-2002	x	x	x	x	x	x
	22	Shear strength	ASTM C273	x	x	x	x	x	x
Combined environments	23	Cryoflex	EQTP 1002 Gradient	x					
	24	Thermal/ Mechanical (1 by 2)	No standard	x	x	x	x	x	x
	25	Thermal/ vibroacoustic		x	x				

Note: Tests marked in grey were previously described and listed in Table 2.
Tests marked in yellow and **bolded** were previously described and listed in Table 2 but additional test conditions were added for the RLV Program.
* Monostrain test determines the derived properties such as ultimate strain, failure stress, Young's modulus, and coefficient of thermal expansion (CTE) in $\alpha\Delta T$.

11. Figures

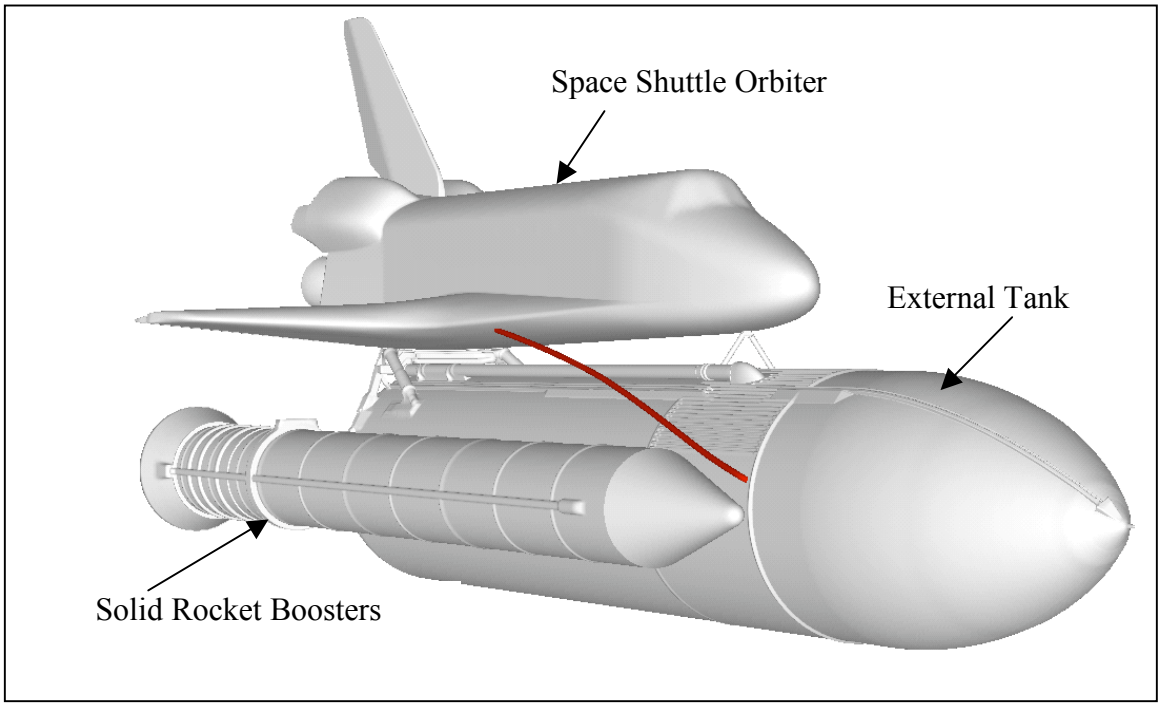

Figure 1. Components of the Space Shuttle Transportation System

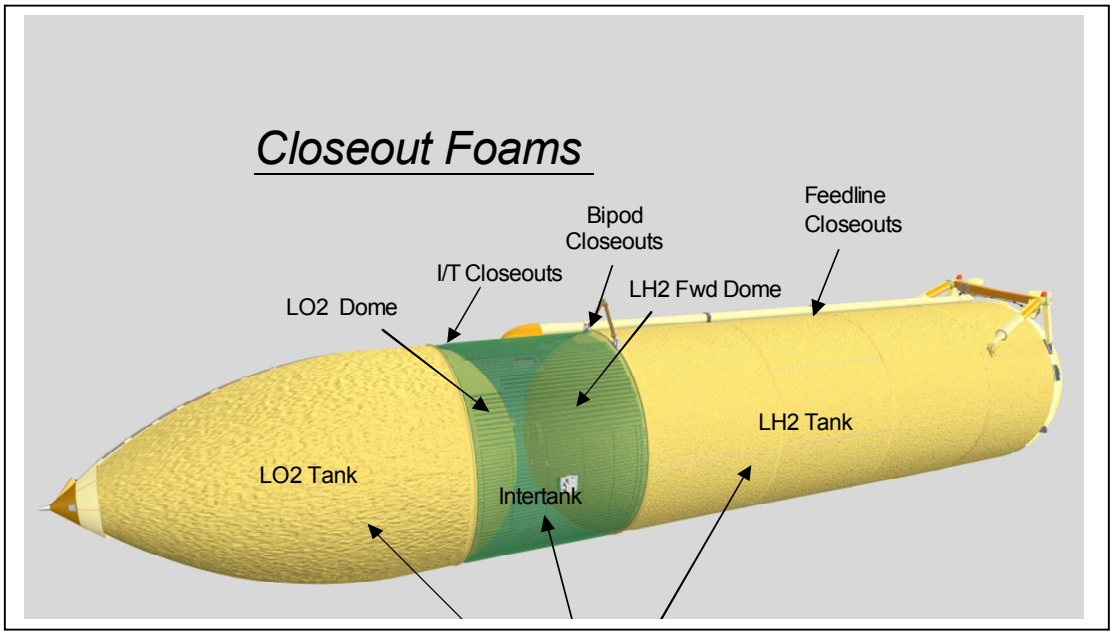

Figure 2. ET components and locations of acreage closeout sprayed foams.

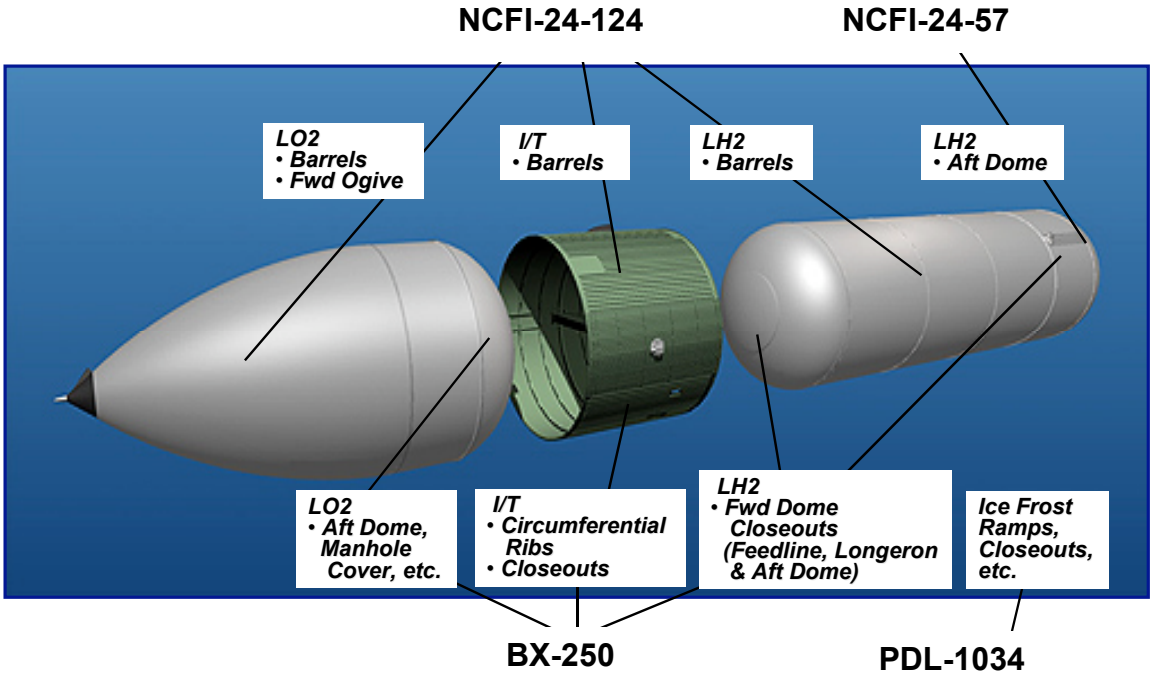

Figure 3. Locations and types of acreage and closeout sprayed on foams for the ET.

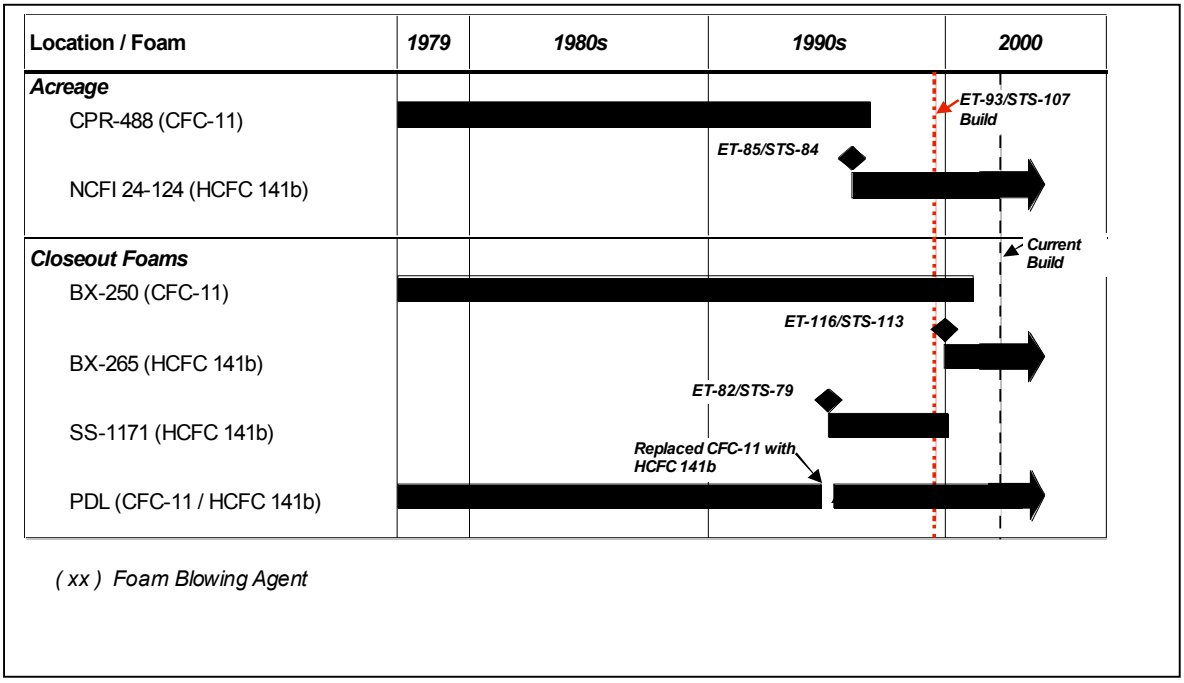

Figure 4. History of the acreage and closeout sprayed on foams for the ET.

			Foam Application		
STS	ET	Completion Date	First Usage	Date	Launch Date
84	85	8/7/1996	LH2 Tank	09/1995	5/15/1997
94	86	10/8/1996	LO2	11/1995	7/11/1997
86	88	1/17/1997	Intertank	12/1995	9/25/1997

Note: STS-107/ET-93 Completion Date: 11/02/2000

Figure 5. Dates of when the acreage sprayed on foam, NCFI 24-124, was phased in for the ET.

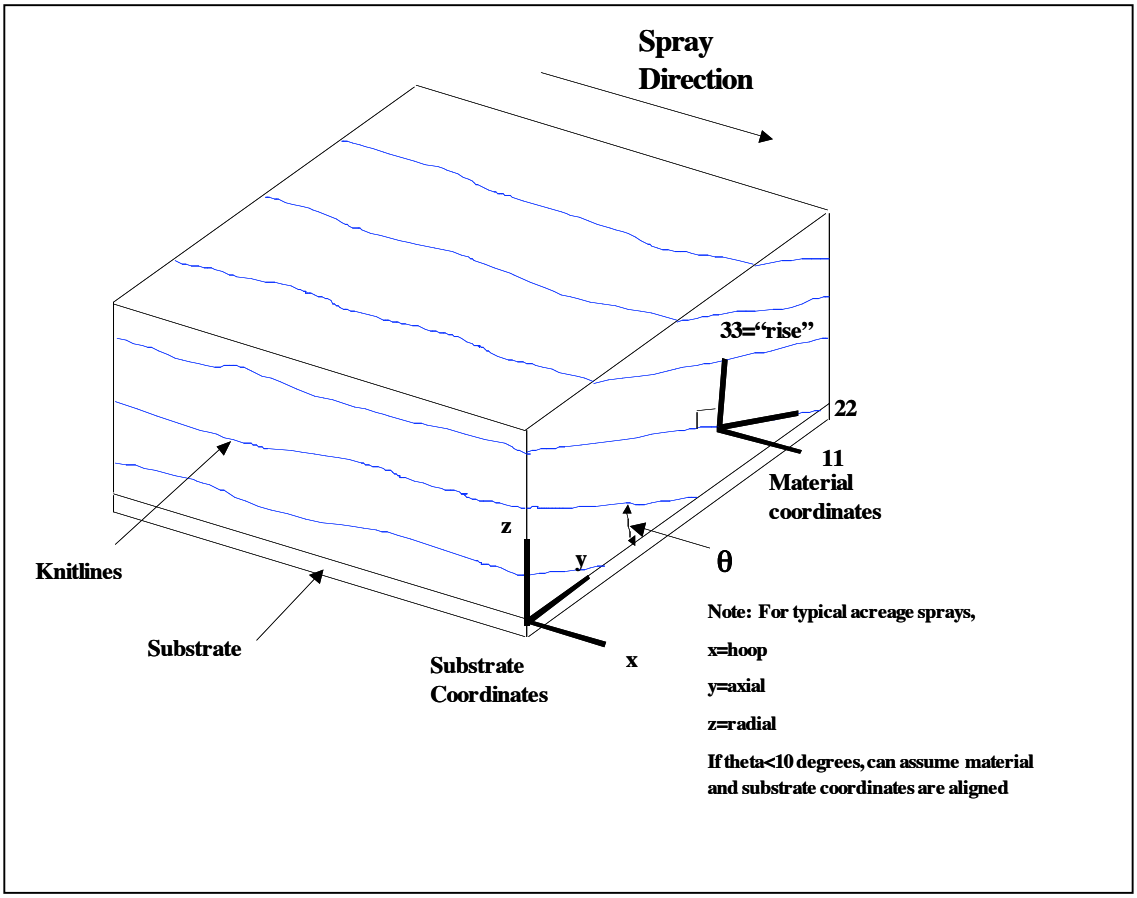

Figure 6. Schematic of typical spayed on foam indicating coordinate directions and knitlines.

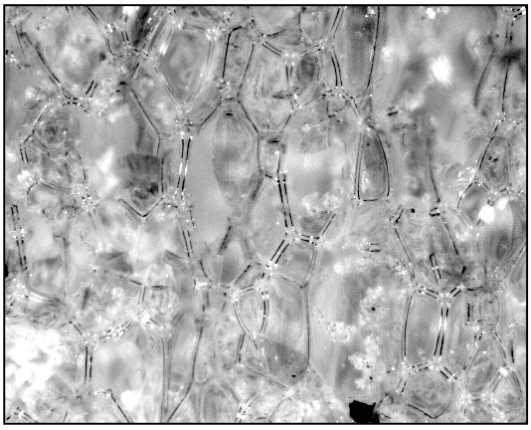

Foam BX-265

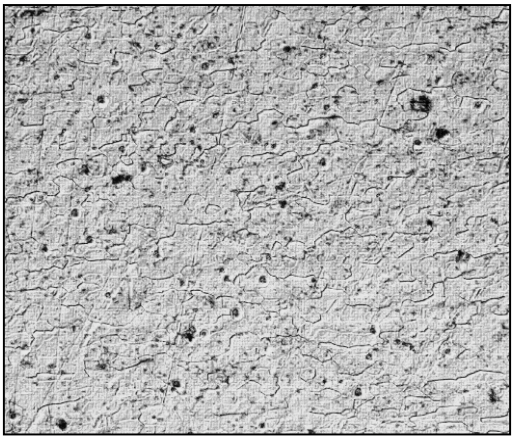

Aluminum

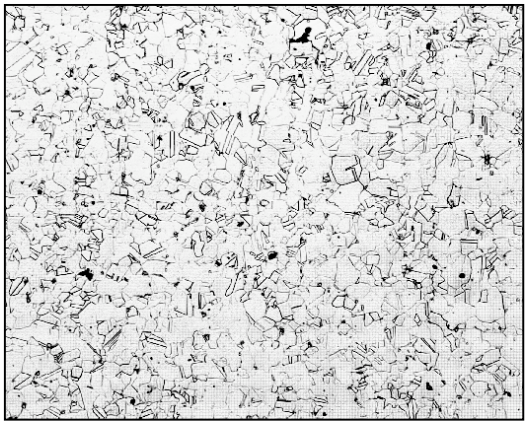

Iconel 625

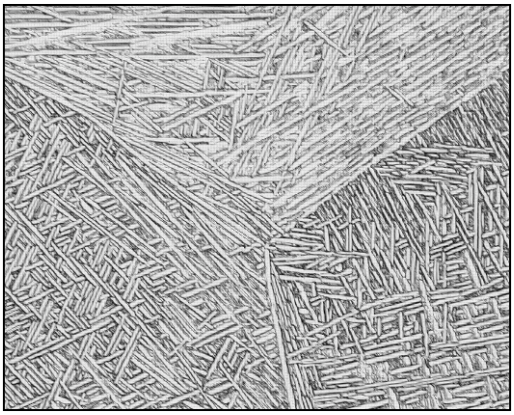

Titanium 6222

Figure 7. Magnified images (50X) of the cell structure of SOFI and morphology of other typical engineering materials.

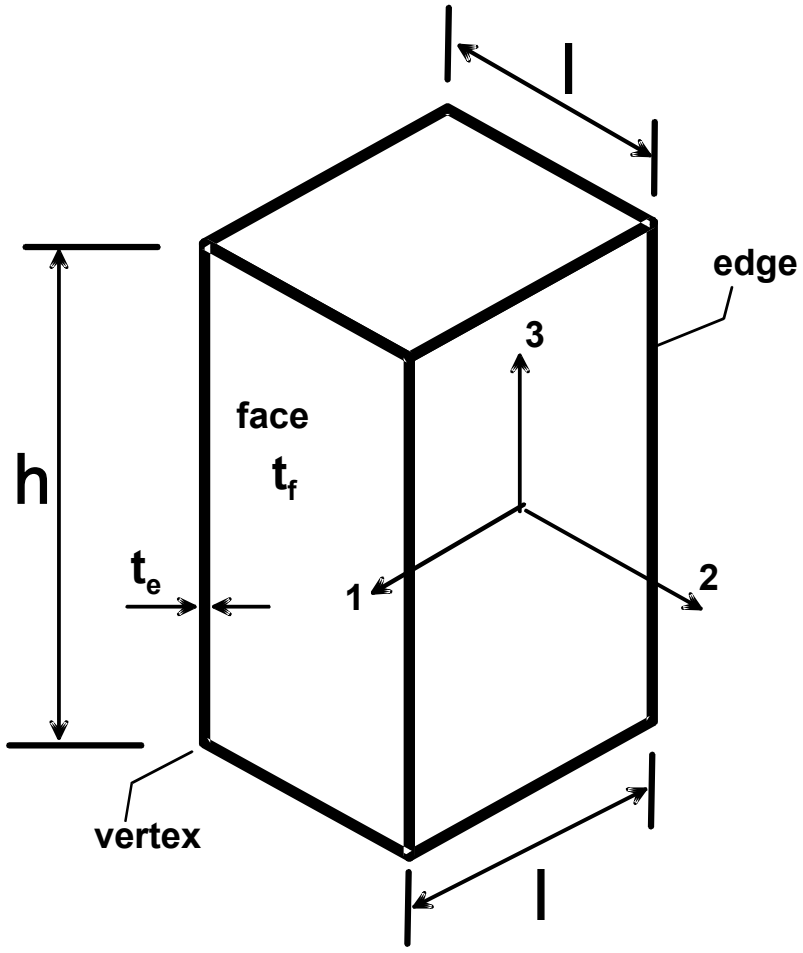

Figure 8. Schematic representation of idealized, rectangular foam cell.

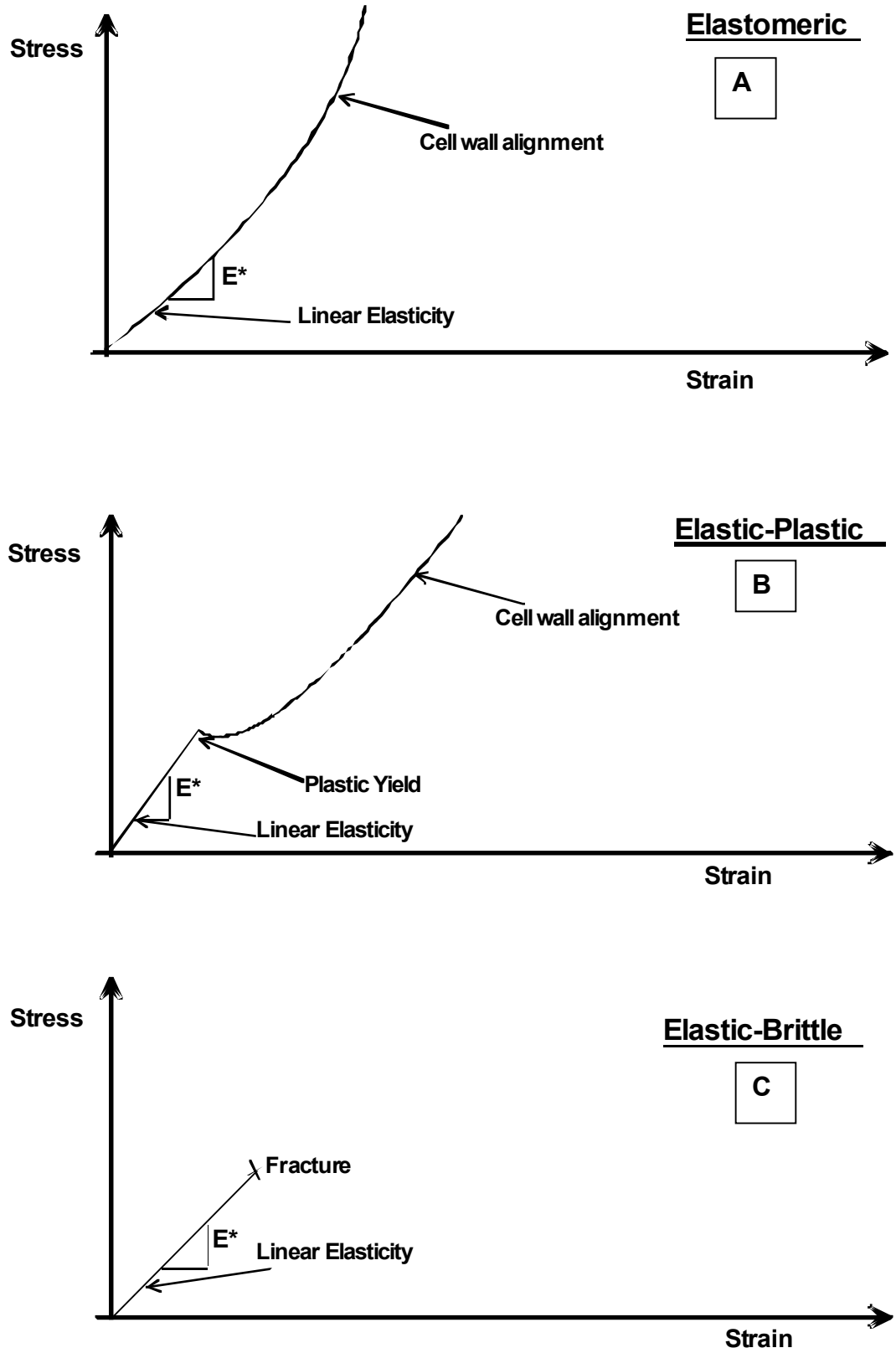

Figure 9. Schematic representation of typical tensile stress-strain curves for closed cell foam.

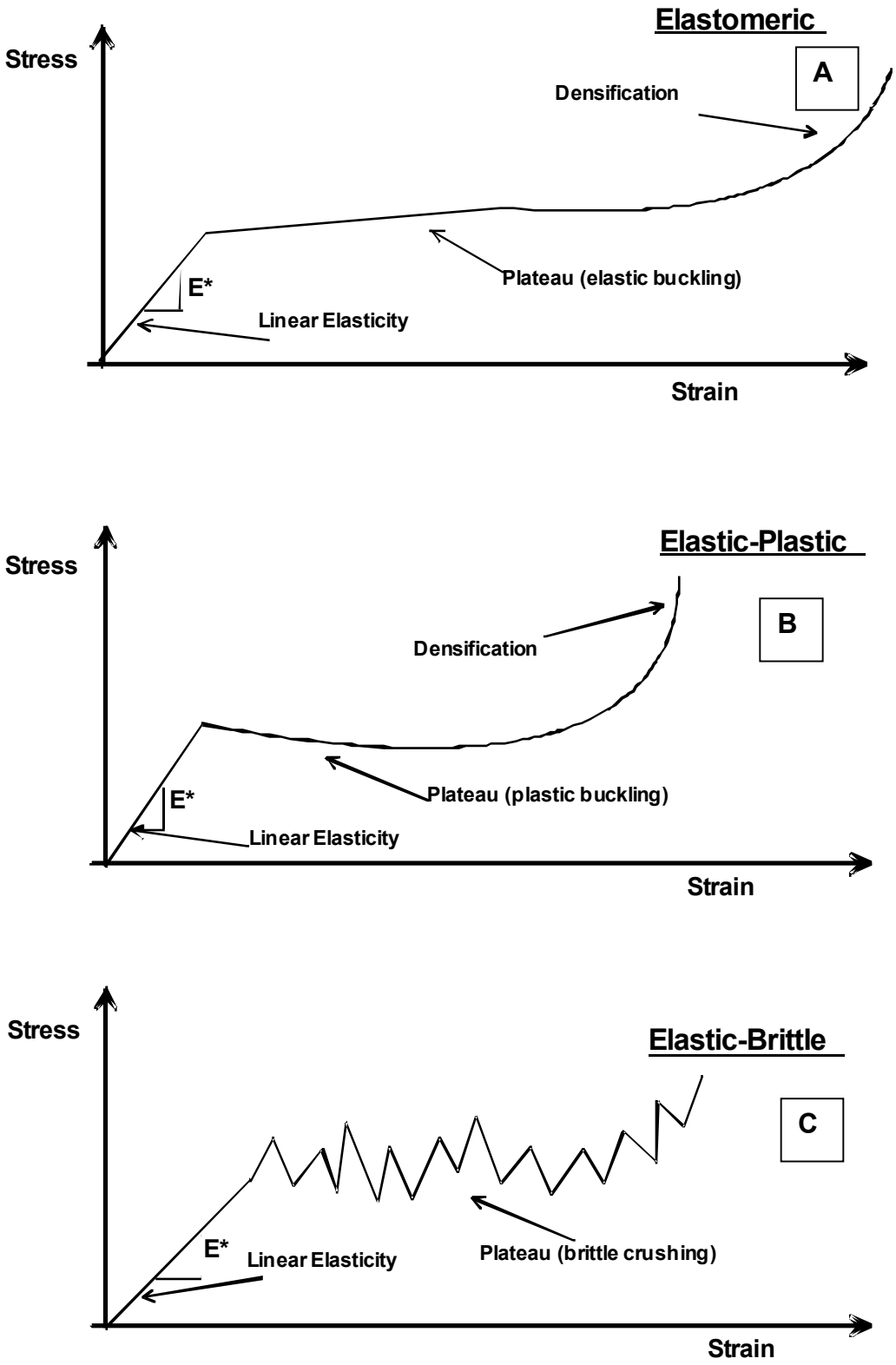

Figure 10. Schematic representation of typical compressive stress-strain curves for closed cell foam.

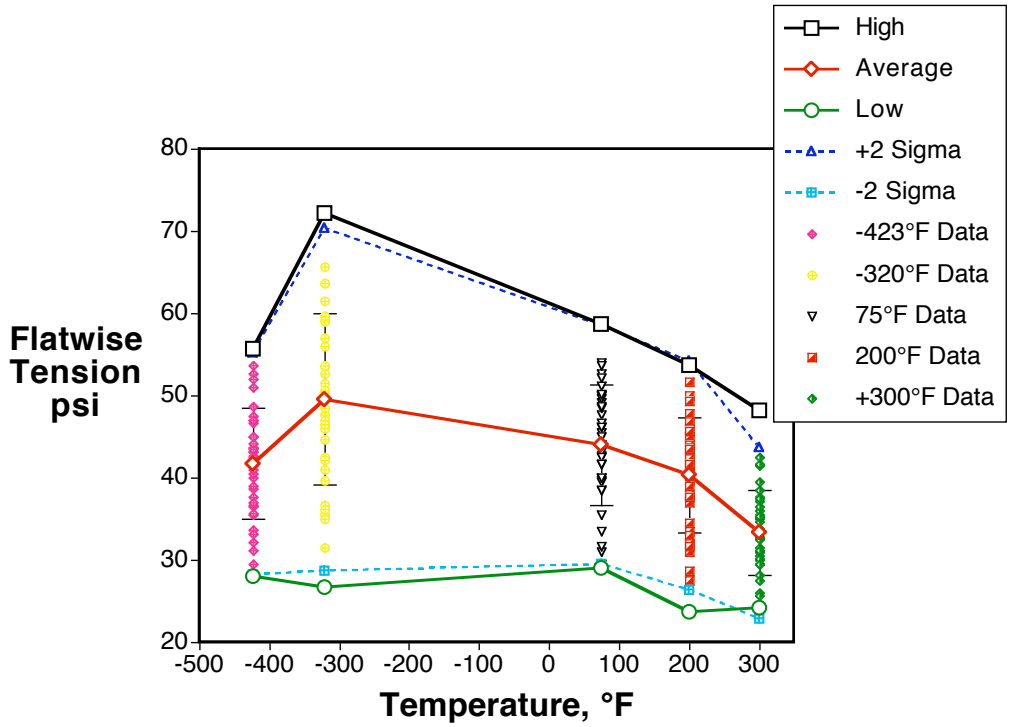

Figure 11. Flatwise tension strength of the NCFI 24-124 illustrating data scatter.

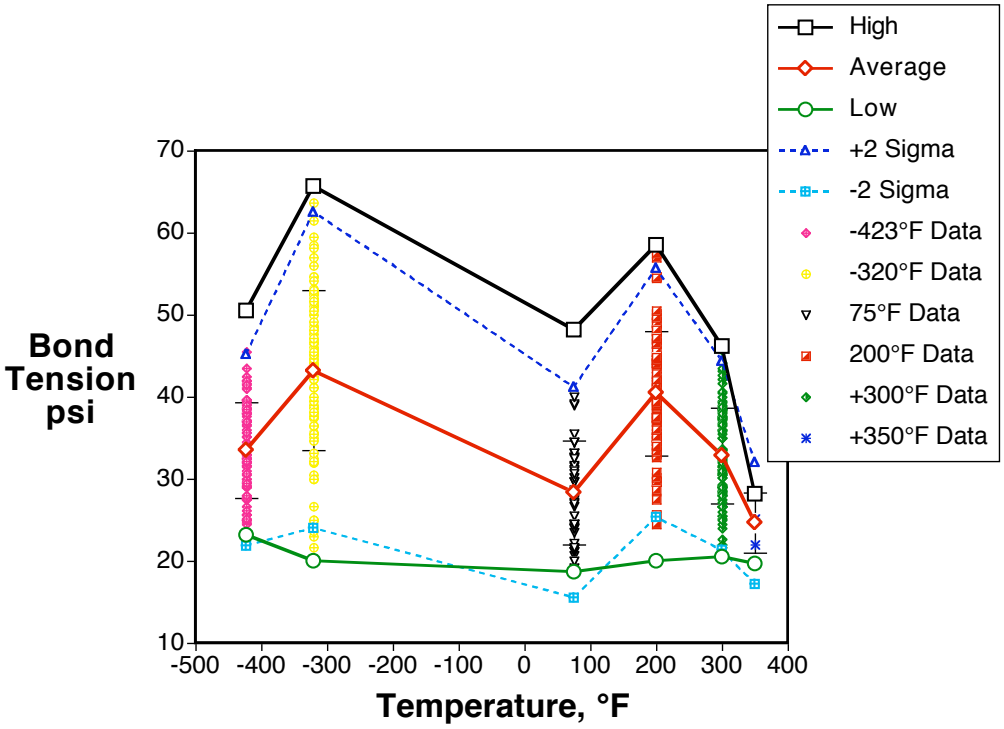

Figure 12. Bond tension strength of the NCFI 24-124 illustrating data scatter.

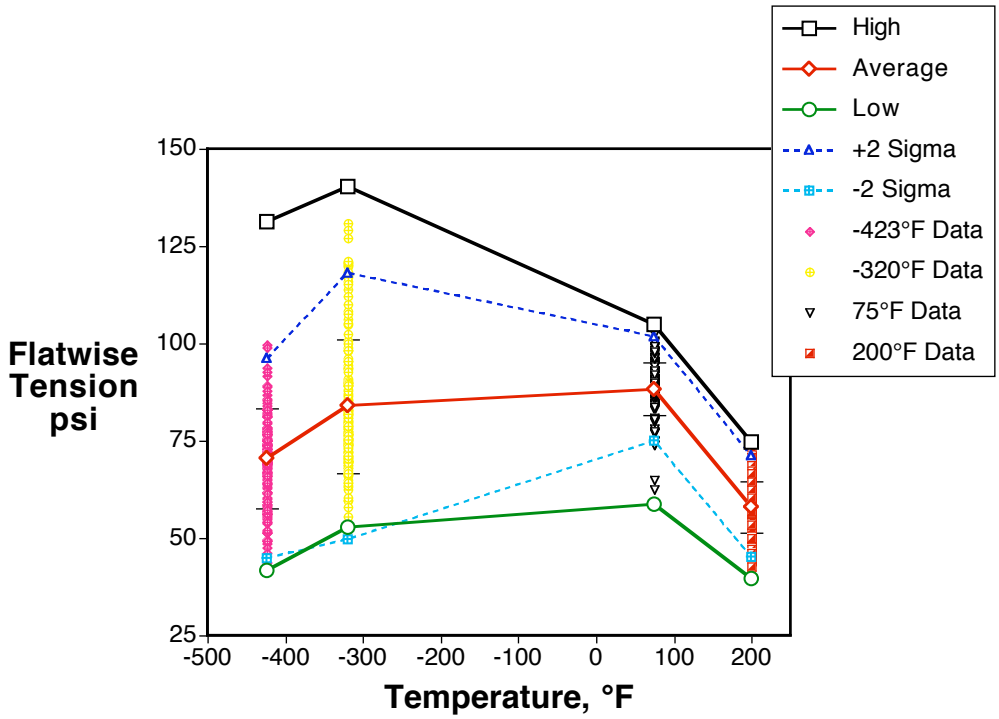

Figure 13. Flatwise tension strength of the BX-265 illustrating data scatter.

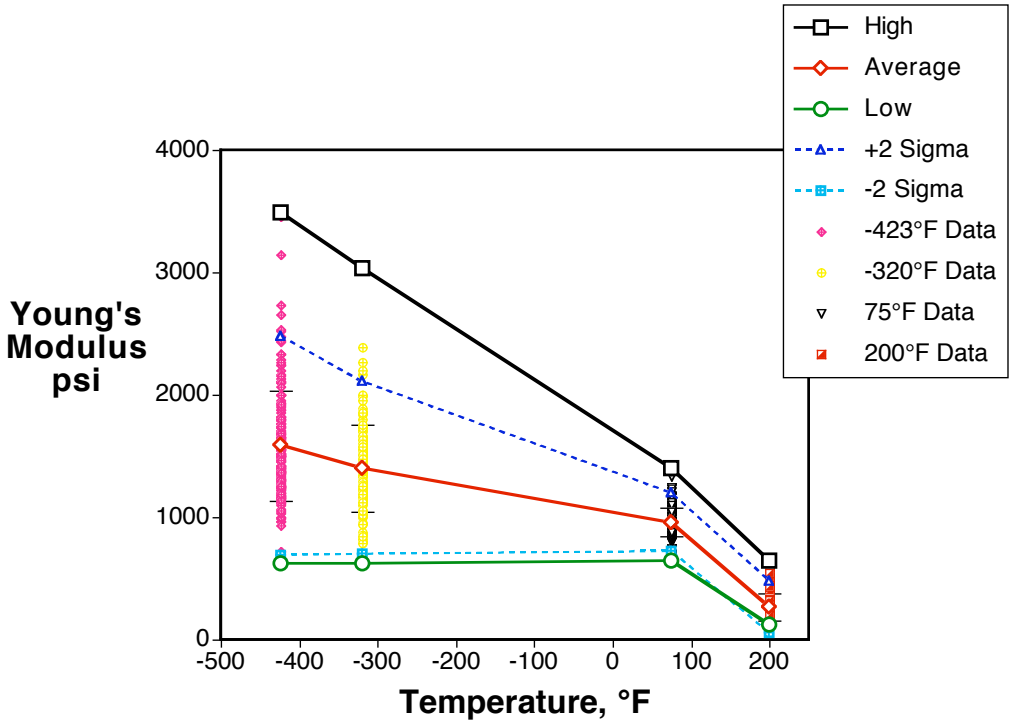

Figure 14. Tensile Young's modulus for the BX-265 illustrating data scatter.

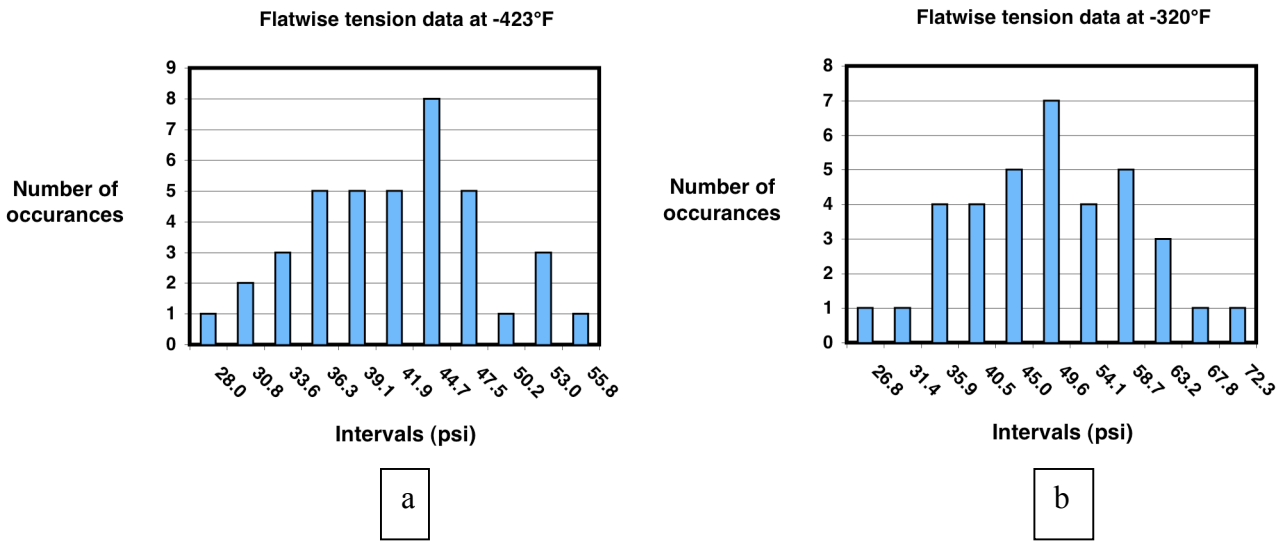

Figure 15. Histograms of the flatwise tension data for NCFI 24-124 acreage foam at a.) –423°F and b.) –320°F.

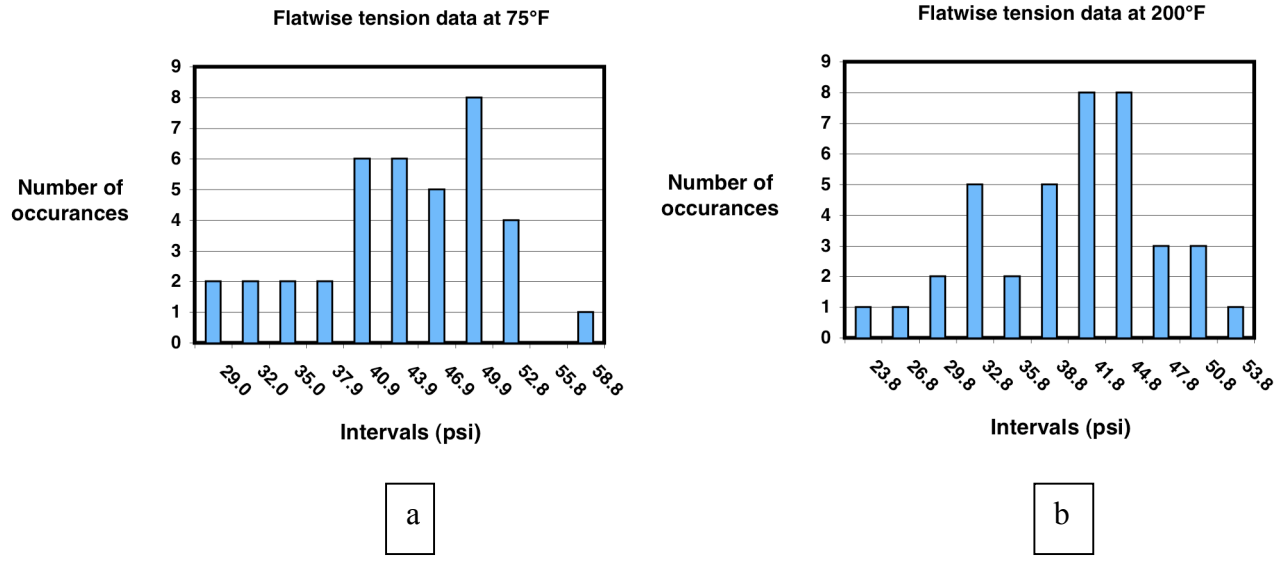

Figure 16. Histograms of the flatwise tension data for NCFI 24-124 acreage foam at a.) 75°F and b.) 200°F.

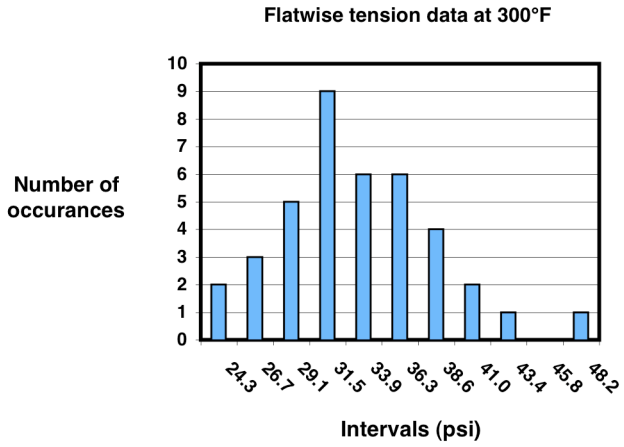

Figure 17. Histogram of the flatwise tension data for NCFI 24-124 acreage foam at 300°F.

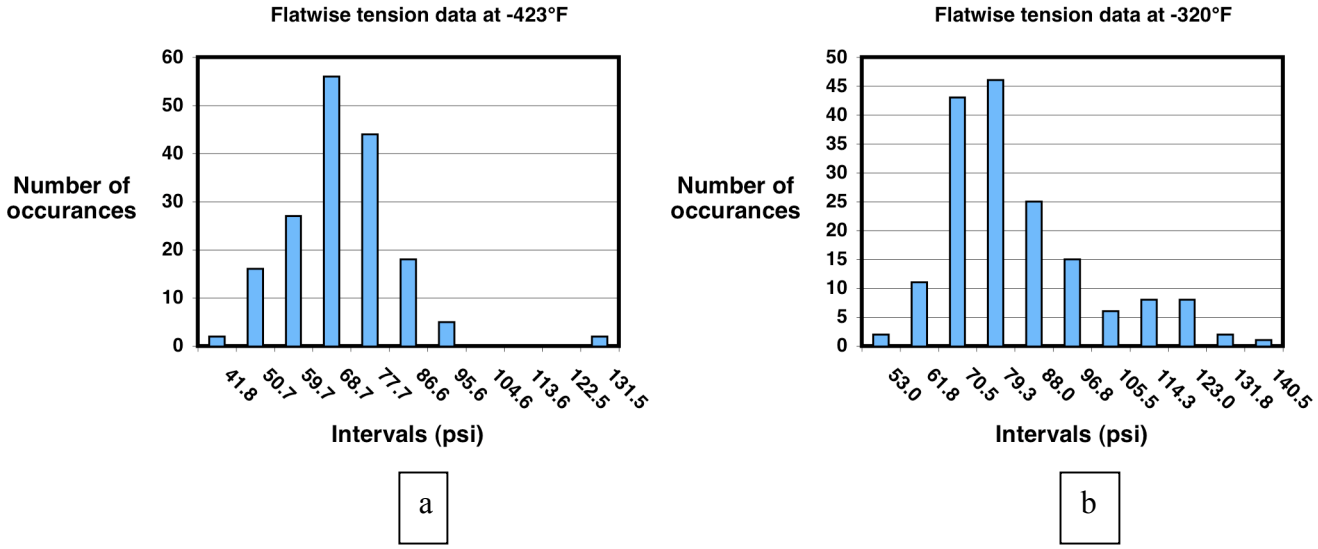

Figure 18. Histograms of the flatwise tension data for BX-265 closeout foam at a.) -423°F and b.) -320°F.

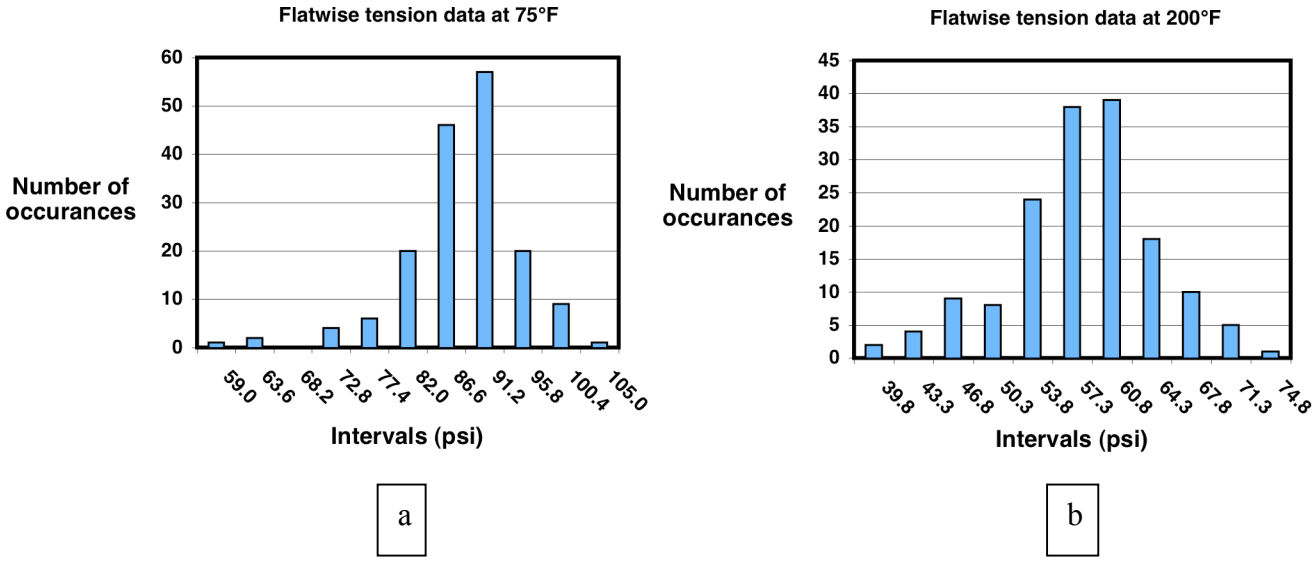

Figure 19. Histograms of the flatwise tension data for BX-265 closeout foam at a.) 75°F and b.) 200°F.

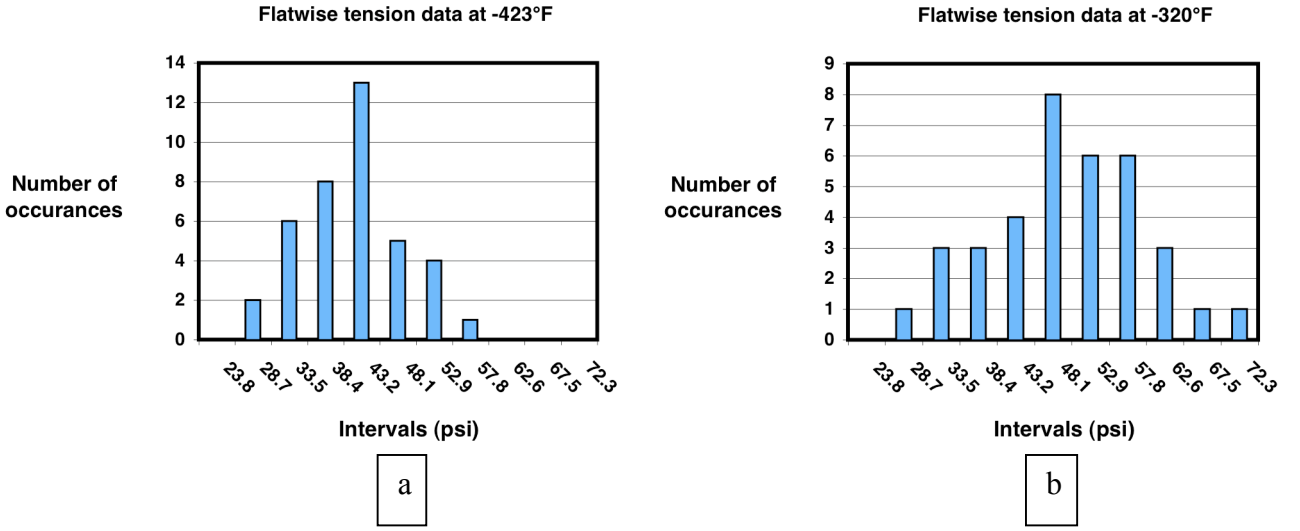

Figure 20. Histograms of the flatwise tension data with a common interval over the entire test temperature range for NCFI 24-124 acreage foam at a.) -423°F and b.) -320°F.

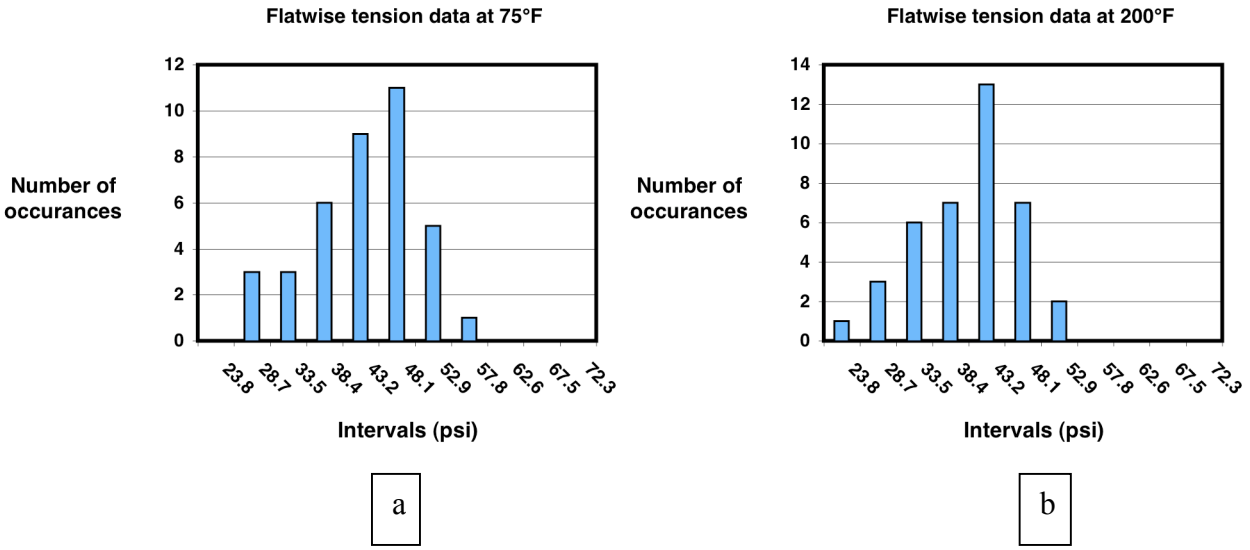

Figure 21. Histograms of the flatwise tension data with a common interval over the entire test temperature range for NCFI 24-124 acreage foam at a.) 75°F and b.) 200°F.

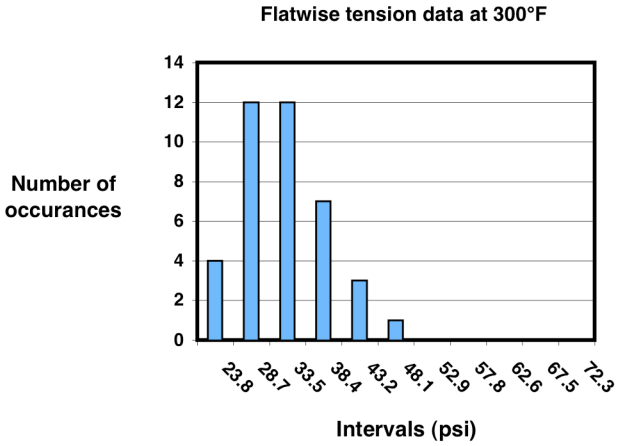

Figure 22. Histograms of the flatwise tension data with a common interval over the entire test temperature range for NCFI 24-124 acreage foam at 300°F.

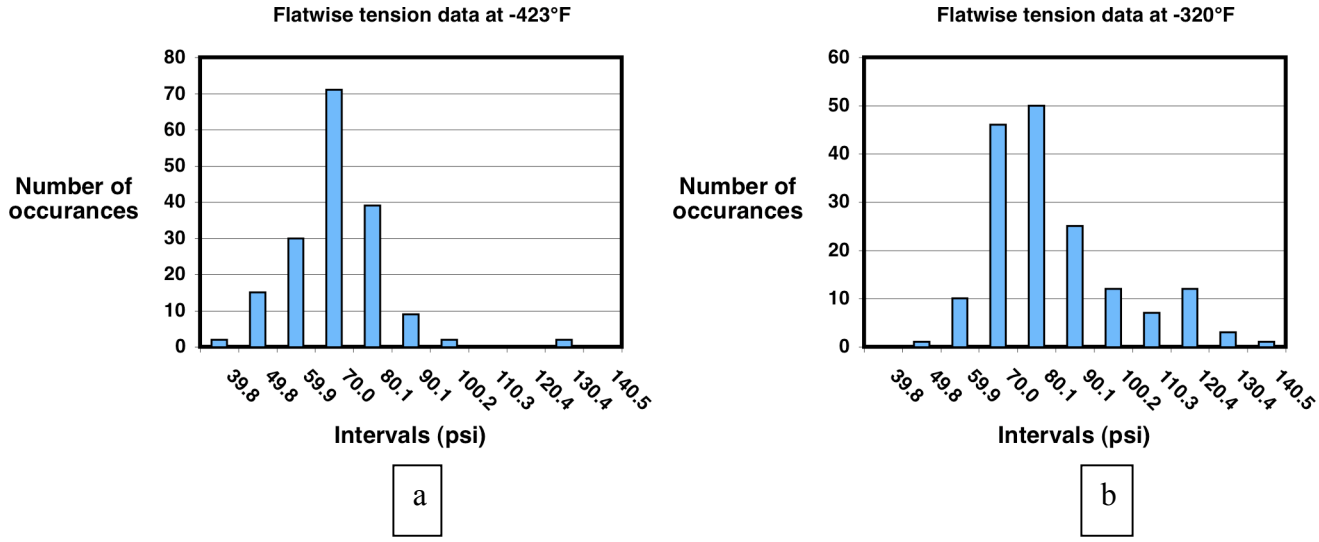

Figure 23. Histograms of the flatwise tension data with a common interval over the entire test temperature range for BX-265 closeout foam at a.) -423°F and b.) -320°F.

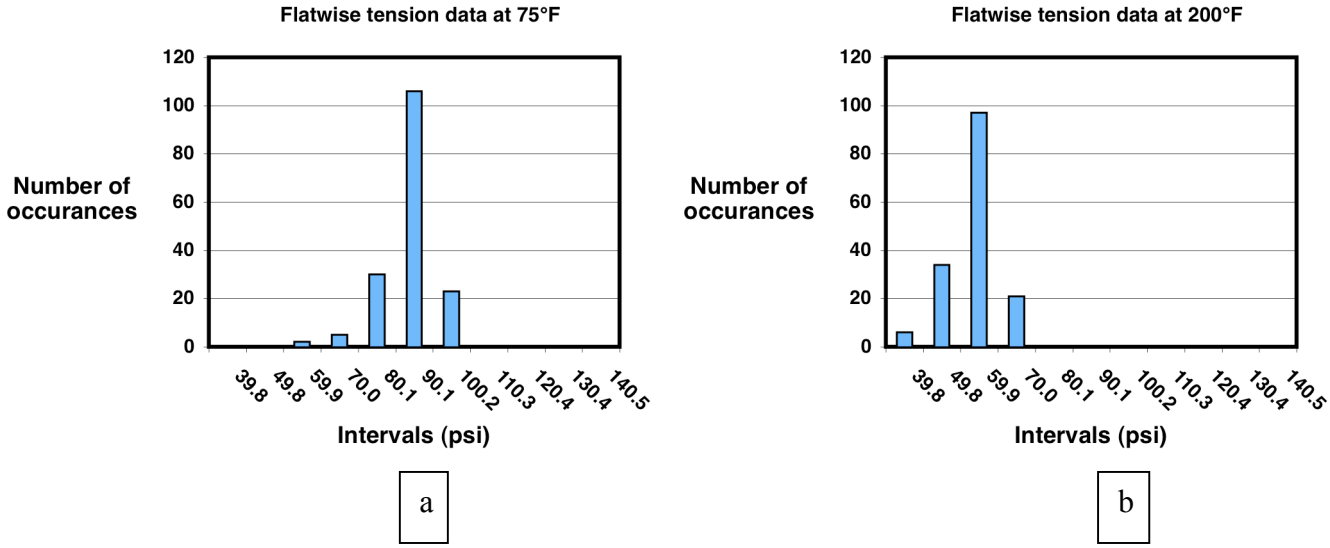

Figure 24. Histograms of the flatwise tension data with a common interval over the entire test temperature range for BX-265 closeout foam at a.) 75°F and b.) 200°F.

REPORT DOCUMENTATION PAGE

Form Approved
OMB No. 0704-0188

1. REPORT DATE *(DD-MM-YYYY)*	2. REPORT TYPE	3. DATES COVERED *(From - To)*
01- 07 - 2005	Technical Memorandum	

4. TITLE AND SUBTITLE

Assessment of Technologies for the Space Shuttle External Tank Thermal Protection System and Recommendations for Technology Improvement

Part 3: Material Property Characterization, Analysis, and Test Methods

5a. CONTRACT NUMBER

5b. GRANT NUMBER

5c. PROGRAM ELEMENT NUMBER

6. AUTHOR(S)

Gates, Thomas S.; Johnson, Theodore F.; and Whitley, Karen S.

5d. PROJECT NUMBER

5e. TASK NUMBER

5f. WORK UNIT NUMBER

23-376-10-30-02

7. PERFORMING ORGANIZATION NAME(S) AND ADDRESS(ES)

NASA Langley Research Center
Hampton, VA 23681-2199

8. PERFORMING ORGANIZATION REPORT NUMBER

L-19147

9. SPONSORING/MONITORING AGENCY NAME(S) AND ADDRESS(ES)

National Aeronautics and Space Administration
Washington, DC 20546-0001

10. SPONSOR/MONITOR'S ACRONYM(S)

NASA

11. SPONSOR/MONITOR'S REPORT NUMBER(S)

NASA/TM-2005-213778

12. DISTRIBUTION/AVAILABILITY STATEMENT

Unclassified - Unlimited
Subject Category 24
Availability: NASA CASI (301) 621-0390

13. SUPPLEMENTARY NOTES

An electronic version can be found at http://ntrs.nasa.gov

14. ABSTRACT

The objective of this report is to contribute to the independent assessment of the Space Shuttle External Tank Foam Material. This report specifically addresses material modeling, characterization testing, data reduction methods, and data pedigree. A brief description of the External Tank foam materials, locations, and standard failure modes is provided to develop suitable background information. A review of mechanics-based analysis methods from the open literature is used to provide an assessment of the state-of-the-art in material modeling of closed cell foams. Further, this report assesses the existing material modeling of closed cell foams. Further, this report assess the existing material property database and investigates sources of material property variability. The report presents identified deficiencies in testing methods and procedures, recommendations for additional testing as required, identification of near-term improvements that should be pursued, and long-term capabilities or enhancements that should be developed.

15. SUBJECT TERMS

Space Shuttle External Tank; Foam Materials

16. SECURITY CLASSIFICATION OF:			17. LIMITATION OF ABSTRACT	18. NUMBER OF PAGES	19a. NAME OF RESPONSIBLE PERSON
a. REPORT	b. ABSTRACT	c. THIS PAGE			STI Help Desk (email: help@sti.nasa.gov)
					19b. TELEPHONE NUMBER *(Include area code)*
U	U	U	UU	67	(301) 621-0390